EFFECTS OF DILUTE POLYMER ADDITIVES ON THE TURBULENCE STRUCTURE NEAR A WALL

Thesis for the Degree of M. S.

MICHIGAN STATE UNIVERSITY

HIROAKI YODA

1981

This is to certify that the

thesis entitled

Effects of Dilute Polymer Additives on the Turbulence Structure Near a Wall

presented by

Hiroaki Yoda

has been accepted towards fulfillment
of the requirements for

MS degree in Mech Engr

R E Falco
Major professor

Date 18 Feb 82

ABSTRACT

EFFECTS OF DILUTE POLYMER ADDITIVES
ON THE TURBULENCE STRUCTURE NEAR A WALL

By

Hiroaki Yoda

When very small concentrations of long chain polymer molecules are added to water, the pressure drop of the flow in a pipe or a channel is drastically reduced. Since the pressure drop needed to drive the flow is required to overcome the resistance the fluid enters, this resistance is reduced by the presence of the molecules. An experimental study was performed with the objective of determining what the effect of the polymer molecules is on the turbulent motion near the wall, which is responsible for the majority of the resistance.

The study focused on determining changes in the length scale and frequency of occurrence of the wall region structure. We have found that the drag reduction resulting from the addition of a polymer is associated with a lower frequency of occurrence of the dominant eddies and a larger length scale for those that develop.

EFFECTS OF DILUTE POLYMER ADDITIVES
ON THE TURBULENCE STRUCTURE NEAR A WALL

By

Hiroaki Yoda

A THESIS

Submitted to
Michigan State University
in partial fulfillment of the requirements
for the degree of

MASTER OF SCIENCE

Department of Mechanical Engineering

1981

ACKNOWLEDGMENTS

I particularly wish to express my gratitude to Dr. R. E. Falco, my major professor, for all his asistance and guidance on this thesis and throughout my M.S. program.

Many thanks to Mr. Barry Berger, who helped me a great deal to construct the flow facility and also to Mr. Brian Leary, Mr. Jeff Lovett and Mr. David Signor for their valuable assistance throughout this work.

Thanks also to all the friends who helped make my graduate studies an interesting experience.

Finally, many thanks to Mr. Hisashi Morita, manager of Pump Design Department of Hitachi Tsuchiura Works, who gave me an interesting chance to study abroad, and also to the people in the Pump Development Group, who supported my study here.

TABLE OF CONTENTS

LIST OF TABLES

LIST OF FIGURES

LIST OF SYMBOLS

b	Spanwise channel width(m)
Deff	Effective hyraulic diameter (m)
Dh	Hydraulic diameter of channel (=(4bh)/2(b+h) , m)
f	Friction coefficient($=4\tau_w/(\rho V_m^2/2)$)
f_s	Friction coefficient for Newtonian flow ($4\tau_w/(\rho V_m^2/2)$)
F	Burst per unit length and unit time ($(m\cdot sec)^{-1}$)
F^+	Non-dimensional burst frequency($=F\nu^2/u_\tau^3$)
$\overline{F}^+$	Mean non-dimensional burst frequency($=F\nu^2/u_\tau^3$)
h	Channel width (m)
K	Non-dimensional pressure gradient parameter($=-dp/dx\cdot\nu/V_c^3$)
M	Dye injection rate($=\dot{Q}_d/(32b\nu)$)
n	Power of power-law velocity profile
N	Occurrence
N_T	Total number of sample
P	Pressure (kg/cm^2)
$\dot{Q}d$	Flow rate of dyed fluid (m^3 /sec)
STD	Standard deviation($=\sqrt{\Sigma(W-\overline{W})^2/(N_T-1)}$, $\sqrt{\Sigma(T_B-\overline{T}_B)^2/(N_T-1)}$)
ReDh	Reynolds number based on hydraulic diameter($=Dh\cdot V_m/\nu$)
Re_θ	Reynolds number based on momentum thickness($=\theta V_c/\nu$)
Res	Reynolds number based on the viscosity of water($=Dh\cdot V_m/\nu$)
t	Temperature of fluid (°C)
T_B	Time between bursts (sec)
T_B^+	Non-dimensional time between bursts($=T_B u_\tau^2/\nu$)

$\overline{T}_B$	Average non-dimensional time between bursts $(=\overline{T}_B u_\tau^2/\nu)$
$\overline{T}_B'$	Average non-dimensional time between bursts $(=\overline{T}_B V_m/(Dh/2))$
u	Local mean velocity (m/sec)
u_τ	Wall shear velocity $(=\sqrt{\tau_w / \rho}$, m/sec)
W	Spanwise width of pockets (m)
W^+	Non-dimensional mean spanwise width of pockets $(=W u_\tau/\nu)$
$\overline{W}^+$	Average non-dimensional mean spanwise width of pockets $(=W u_\tau/\nu)$
wppm	Part per million by weight
V_c	Veocity at the center line of channel (m/sec)
V_m	Mean velocity in channel (m/sec)
x	Streamwise distance from dye slit (m)
x^+	Non-dimensional streamwise distance from dye slit$(=X u_\tau/\nu)$
y	Distance from the wall (m)
y^+	Non-dimensional distance from the wall$(=y u_\tau/\nu)$
z	Spanwise distance (m)
z^+	Non-dimensional spanwise distance$(=z u_\tau/\nu)$
α	Facter of shear stress$(=(\tau-\tau_w)/y)$
θ	Momentum thickness$(=\int_0^{h/2} u/V_c(1-u/V_c)dy$, m)
λ	Streak spacing (m)
λ^+	Non-dimensional streak spacing $(=\lambda u_\tau/\nu)$
$\overline{\lambda}^+$	Average non-dimensional streak spacing$(=\overline{\lambda} u_\tau/\nu)$
ν	Kinematic viscosity (m^2 /sec)
ν_w	Kinematic viscosity of water (m^2 /sec)
τ	Local shear stress (kg/m^2)
τ_w	Wall shear stress (kg/m^2)

ρ Density (kg/m^3)

Δ_τ Non-dimensional shear stress gradient ($=\alpha \cdot \nu/(\rho u_\tau^3)$)

$+$ Non-dimensional form by the wall coordinate (u_τ, ν)

$'$ Non-dimensional form by the outer layer flow coordinate (Vm, Dh/2)

$-$ Mean sample ($= \Sigma W/N_T$, $\Sigma T_B/N_T$)

CHAPTER 1

INTRODUCTION

The phenomena of drag reduction through the addition of small quantities of polymer molecules has great potential to be able to reduce the consumption of energy which is a crucial problem in our society.

There have been many studies of the effects of dilute solutions long chain molecules on the flow fields since the discoveries by Mysels and Toms from 1945 to 1946. An important aim of these studies is to determine the mechanism of drag reduction in pipe or channel flows.

Lumley (1969) defined the drag reduction as the "reduction of skin friction in turbulent flow below that of the solvent alone". These studies show that the mechanism of drag reduction in pipe or channel flows results from a modification of the turbulence. Hence, it can be understood on the basis of the structure of turbulent flows.

The structure of any turbulent flow reflects the local balance of production, transport and dissipation of turbulent kinetic energy. In turbulent flows bounded by walls the production of new turbulence near the walls plays a primary role in the flow dynamics. The region of important turbulence production is usually rather thin and located very close to the wall, and therefore difficult to investigate. Our knowledge of the changes that occur is far from sufficient to understand the phenomena.

The extensive visual studies of Newtonian turbulence structure have been reviewed by Kline (1978). Probes studies have been reviewed by Willmarth (1975). Combining results both from visual and quantitative techniques reveals a number of significant features of turbulent boundary layers.

First, the sublayer is not two-dimensional and steady, rather it contains three-dimensional unsteady motions. While the motions in this region are indeed dominated by viscosity, "eddy" motions are present throughout the entire wall region. Secondly, it appears that a primary mechanism for production of turbulent kinetic energy in the inner region of the boundary layer is the rather rapid movement towards the wall of high speed fluid and the violent ejection of low-speed fluid from the regions very near the wall. These "bursts" are highly suggestive of an instability mechanism, and also appear to play a key role in transporting turbulent kinetic energy to the outer regions of the boundary layer.

From 1959 to 1967, Kline and his co-workers, by seeping dye through the wall under a turbulent boundary layer and using hydrogen bubble flow visualization, showed that streaks formed, presumably by the action of streamwise vorticity. These streaks were not only inherent to the sublayer of the turbulent boundary layer under a variety of flow conditions, but also played a very important role in the turbulence production. The streaks are not observed using the same technique in laminar boundary layers. The data indicated that the averaged spanwise streak spacing corresponds approximately to $\bar{\lambda}^+=100$, which is 15-20 times the thickness of the viscous sublayer. Hence, this appears to be a characteristic scale of motion within the wall regions, and the scaling suggested that it is determined primarily by the wall-region parameters. Their measurements also yielded the average dimensionless frequency of streak breakup ($\bar{\omega}^+=2\pi \bar{F}^+\bar{\lambda}^+$) which equals about 0.06 for the flat plate zero pressure gradient flow.

From 1972 to 1978, using a similar dye visualization technique, Tiederman and his co-workers obtained new evidence which suggested that a significant mechanism by which a dilute polymer solution achieves drag reduction is by inhibiting the formation of the streaks. At equal flow rates the smaller number of streaks in the drag reducing flow yields a lower spatially averaged bursting rate, less turbulent momentum transport, and hence a reduced wall shear stress.

The search for mechanisms for the production of turbulence near a wall has resulted in a large number of semi-empirical models. Townsend in 1956 (see Townsend 1976), Blakewell and Lumley's (1967) models consist principally of streamwise oriented vortices which are attached to the wall. From space-time correlation measurements Blakewell and Lumley found the correlation of streamwise velocity (U) over 40 viscous lengths, suggesting that the vortices are well correlated over this length. However, these studies were not able to determine the mechanism of formation of the streaky structure, or the mechanism of break-up of streaky structure.

Recently, high resolution visual investigations of the flow in the wall region performed by Falco and his co-workers (1977-1981) indicated that the production of turbulence takes place as a result of the interaction of coherent eddies of the outer flow with the wall. The outer layer eddies which were important were microscale sized eddies rather than large scale eddies, which were postulated by many authors as possible excitors of the sublayer structure. The footprints of these interactions result in an array of pocket patterns in the visualized sublayer.

Falco (1980) also showed that the pattern is the most important wall region structure, suggesting that the scales of the pocket were closely related to those reported already for other indications of important wall region events. It is found that the pocket pattern appeared both when the long streaky structure brakes-up as well as in between the long streaks.

Falco (1980) broke down the pocket evolution into five stages. Figure 1.1 shows the sketches of visualized pocket pattern with side view sketches (which were obtained by a laser sheet visualization) for several of the stages with indications of the vortices found present.

At the first stage, pockets are formed by high speed fluid which comes toward the wall (this is called a sweep). Stage two is characterized by the formation of the characteristic crescent shape in the marked sublayer. Flow visualization at this stage indicates the lift-up of sublayer fluid and its rotation about a vortex which is apparently formed or amplified along the boundary of the cresent shaped pockets. The pocket pattern of stage three becomes pointed at its upstream end and elongated. The stream-wise velocity perturbation begins to show the formation of a region of low velocity forming a little bit downstream of the pocket pattern. At stage four, the region of velocity defect downstream of the pocket pattern continues to increase, forming a hairpin-like vortex there. Stage five leaves the visual impression of the pocket pattern distorted. An orderly ejection which started at stage three becomes chaotic with all indications of vortices and any other sense of coherence disappearing. The last stage may correspond to the instability mechanism which Kline (1967) mentioned concerning to the breakup of streaks, though it is not still clear how the instability is triggered.

However, pocket pattern observed by Falco (1977) in the sublayer of boundary layers had not been seen in pipe or channel flow. The expected similarity of the wall region structure of boundary layers and pipe or channel flows suggests that pockets should exist in pipe or channel flows, but high resolution investigation would be required to resolve these features.

By studying the length scales and frequency of occurrence of the pocket pattern, it should be possible to determine the effect of polymer additives on the wall layer flow. This investigation was aimed at finding changes of these length and time scales when polymers are added to channel flows.

CHAPTER 2

DESCRIPTION OF EXPERIMENTS

2-1. Flow facility

The experimental study was conducted in a rectangular channel and a skematic of the flow system is shown in figure 2.1. The channel sides are made of single continuous sheets of transparent plexiglas, 2.37 meters long and 38.1 mm high and 209.6 mm wide, with a hydraulic diameter of 64.5 mm. The flow from the reservoir of water to the beginning of the channel is designed so as to prevent flow disturbances and high shear. That is, a bellmouth and an expansion channel with 12.6 degrees are used at the bottom of the reservoir and at the entrance of the test channel respectively. A 2 mm trip placed on all four walls of the channel was used to ensure fully turbulent flow.

All flow visualization experiments were done by using only the potential energy of water in the reservoir. This "once through" flow system, combined with the low shear entrance conditions, helped to keep polymer degradation to a minimum.

Polymer degradation affects drag reduction in a poorly-defined manner, and is partly responsible for the large scatter and conflicting results of many previous investigations. The capacity of the reservoir enables experiments of 20 to 40 second duration. In order to a obtain constant velocity flow in the channel during each run, the float-pulley system shown in figure 2.1 is employed. The system can provide constant difference of height between the surface of water in the reservoir and the outlet of the flexible tubing. The flow rate is controlled by the ball valve.

2-2. Flow rate and wall shear measurement.

The velocity was calculated from the flow rate which was obtained during each run by determining the time interval required to collect a quantity of fluid in a catch reservoir.

The ball valve employed to control flow rate was opened and shut quickly enough to count the running time of fluid without losing accuracy of measurement. The accuracy of velocity obtained in this way was no more than 4%. The wall shear and shear velocity were calculated from measurements of pressure difference between two 3.0 mm diameter wall pressure taps. The upstream pressure tap was 1534 mm downstream of the entrance of the test channel while the downstream pressure tap was 292 mm upstream of the exit of the test channel. A two-fluid micromanometer consisting of water above carbon tetrachloride was used to measure the pressure difference. The micromanometer had resolution of 0.03 mm. The average wall shear stress was calculated directly from the pressure difference measurements (see Appendix B). The wall-shear velocity (u_τ) was calculated from its definition using the density of the experimental fluid. The friction coefficient (f) (Appendix B), calculated from the pressure difference and the flow rate measurements were compared with available data of friction coefficient for pipe flows and channels flows. Results of water experiments in the test channel are shown in figure 2-2 where the friction coefficient is plotted as a function of the Reynolds number based on the average velocity Vm and hydraulic diameter Dh. The variation of the test channel data are within the accuracy of the measurement techniques, and in reasonable agreement with the equation for rectangular channels given by White (1979), which enables us to predict the turbulent friction coefficient of rectangular channel flows most accurately when an effective diameter Deff equal to 0.64 times the hydraulic diameter Dh is employed.

2-3 Dilute polymer solutions

Each batch of polymer solution was prepared from a 2000 wppm concentrated solution which was mixed in a separate 0.11 m tank. The concentrated solution was held in this tank for 48 hours to provide enough time for hydration.

Dilution and thorough mixing to the desired 100 wppm concentration solution was done in other 0.11m tank. This method of mixing gave clear homogeneous solutions without any visable agglomerations.

As a high-molecular-weight polymer, Separan AP273 (mean molecular weight 9×10^6) made by the Dow Chemical Company was used (see Appendix D). The kinematic viscosity data for Newtonian and dilute polymer were employed from the references Kays (1980) and Oldaker and Tiederman (1977) respectively. Especially careful attention was paid in terms of solution temperature and mixing process to make dilute polymer solutions similar to those in the above references.

2-4. Flow visualization technique and motion picture analysis

Visualization of the near-wall region was accomplished by seeping dyed fluid through a wall dye slit located 1969 mm downstream of the test channel entrance. The slit configuration is shown in figure 2.3. The dimensions of the slit are 100 mm in the spanwise direction and 0.1 mm of gap clearence through which the dyed fluid entered the test channel.

The dye slit and the test channel made from a continous sheet of plexiglass, allowed us to minimize flow disturbances, and to identify the two-dimensionality of the test channel and the Reynolds number for laminar to turbulent transition in the test channel. At Reynolds numbers low enough for laminar flow to exist in the channel, the dye sheet eminating from the slit was very uniform and it remained undisturbed and close to the wall all the way to the channel exit. When the Reynolds number was raised between 8000 and 10,000, the dye sheet formed streaks which fluctuated randomly, though pocket patterns were not observed in movie pictures. These experiments indicated that for ReDh>10,000 the flows were fully-developed turbulent channel flow. Hence, all of experiments were conducted at ReDh>10,000.

One of the most important consideration in the use of the dye visualiqation technique is the injection rate of dye. However, in this matter Oldaker and Tiederman (1977) reported that the streak spacing was not affected significantly by the injection rate of dye, M, more than 1/27 for both Newtonian and dilute polymer solution flows. Hence, in this experiment, the height of the dye reservoir was set to provide dyed fluid which gives an injection rate "M" of 1/2 - 1/3 (Appendix C).

The due was prepared from a 0.1% solution of rhodamine B, a water soluble fluorescent dye whose color is red. It is made by the Eastman Kodak Company. In the dilute polymer solution experiments, the dye solution was prepared from the same batch of polymer solution used in the experiment.

The motion pictures were made with a Locam 16 mm camera with a 25 mm lens fitted with three close-up diopters. The framing speed was set at 100 frames per second which allowed us to observe the evolution of pocket pattern as discussed in the introduction. The camera was mounted above the test channel to take top-view pictures just downstream of the dye slit, because pocket pattern is observable more clearly there than farther downstream of the dye slit. This is due to the fact that there is amore uniform distribution of dye on the wall. Two flood lights (total 800 watts) were used for illumination. A white color thin polyester sheet was adhered by glue on the wall surface to provide a clear contrast with the red dye. Kodak 162R7605EI film was used.

Objective analysis of the motion pictures was one of the most important matters. There are many factors which influence the quality of pictures. Lighting technique, processing of film and dye injection rate all seriously effected the quality of the visualization. Hence, these factors were kept as constant as possible during experiments both for Newtonion and dilute polymer flows.

Once the quality of the visualization was optimized, the problem of pocket discrimination remained. The discrimination needs for length scale determination differed from those of the frequency of occurrence. The discrimination criteria used in this experiment is discussed next. The counting method to determine the frequency of occurence is shown in figure 2.4. The pockets in all stages of their evolution (figure 1.1) were counted when they crossed the measuring station which was about $x+=100$ to 200 downstream of the dye slit. The pockets were difficult to observe farther downstream from the dye slit because most of the dye had been convected away from the wall, and that which remained marked a relatively small portion of the wall in the streaky structure. In order to build up a large enough sample of pockets, usually three measurement positions, all at the same distance from the slit were used. They were more than $z+=200$ apart, so that the pockets detected at each of these measuring positions provided independent data for the ensemble average. At each position, the frame number at which pockets intersected the cross-hairs was recorded, from which the intervals of pockets appearance at the measurement positions were calculated.

The criteria used to obtain length scale was to measure the pockets at their maximum width of pocket which has reached fully-developed stage III. A number of criteria are possible. The criteria adopted here was to measure the spanwise distance between the densely marked streaks. The analysis of the motion pictures was done from the back side of a ground glass screen on which the films were projected. Finally, the average interval ($\overline{T_B}$) of pocket occurrence, and the average width ($\overline{W}$) of pockets were reduced to non-dimensionalized form.

For (T_B) and (W), the non-dimensionalized forms are ($T_B \cdot u_\tau^2/\nu$) and ($W \cdot u_\tau/\nu$) respectively, where u_τ is the wall shear velocity and is the kinematic viscosity of fluid. The standard deviations for (T_B) and (W) are calculated where S.T.D.T.=($\sqrt{\Sigma(T_B - \overline{T_B})^2/(N_T - 1)}$) and S.T.D.W.= ($\sqrt{\Sigma(W - \overline{W})^2/(N_T - 1)}$) respectively where N_T is the total number of samples. Movie pictures were taken at three different Reynolds numbers between 10,000 and 20,000 for Newtonian flows and for dilute polymer flows. The data were plotted both in terms of both the Reynolds numbers ($R_{e\theta}$)

based on the momentum thickness of the boundary layer and the velocity along the centerline of the test channel, and the Reynolds number(R_{eDh}) based on the hydraulic diameter. The technique used to convert from (R_{eDh}) to (Re_{Θ}) is given in Appendix A.

2-5. Accuracy of Measurements

The overall accuracy of measurements is shown in Table 2-1 where these overall accuracies don't include the accuracy of the frequency or length scale measurements. The calculation of these accuracies is shown in Appendix E.

CHAPTER 3

RESULTS

Figure 3.1 shows the friction coefficient (f) both for Newtonian flows and for dilute polymer flows. It should be noted that the Reynolds number (ReDh) for the dilute polymer experiments is based on the kinematic viscosity of the polymer solution instead of the solvent Reynolds number (Res).

The friction coefficient (f) for the dilute polymer flows shows the marked decrease compared to that for water. The maximum drag reduction defined as $(f_s - f)/f_s \times 100\%$ which has been obtained in this range of Reynolds numbers is about 40% on the basis of (ReDh) or about 36% on the basis of the solvent Reynolds number (Res). The onset of drag reduction occurred at about (ReDh)=11,000. In terms of the wall shear velocity (U_τ) the wall shear velocity at the onset corresponds to (U_τ)=0.017m/sec. The author is not aware of data of onset wall shear velocity for AP273. However, this datum seems to be correlated well with the data of the onset wall shear velocity (U_τ)=0.024m/sec given by Peterson (1973) for AP30 which is chemically similar to AP273 but has lower molecular weight ($M=2.0\times10^6$) because a decrease in the dimensions of a macro-molecular random-coil in solution increases the onset wall shear velocity as discussed by Virk (1975). It should be noted here that the fluctuation of flow was much lower in dilute polymers flows than in Newtonian flow. It is likely that this lower fluctuation flow gives less scattered data of the friction coefficient in dilute polymer flows than in Newtonian flows.

A summary of the experimental results is given in table 3.1. Figures 3.2 and 3.3 show representative pictures of pockets taken from the movies. The pocket shapes and evolution observed in the channel flow both for the Newtonian flows and the dilute polymer flows appeared similar to the pockets found in the turbulent boundary layer. The appearance of pockets as the dominant flow structure not only in the boundary layer but also in the channel flow shows that the expected similarity of turbulence structure exists near the wall.

The length scales of the pocket pattern obtained from both the Newtonian flows and the dilute polymer flows are presented in figure 3.4 where they are compared to the results of the streak spacing by Oldaker and Tiederman (1977).

Histograms of the length scale measurements both for the Newtonian flows and the dilute polymer flows are presented in figure 3.5. Results calculated from the pockets at Stage III, and at all stages are shown. The measurement of pockets at Stage III has too small a sample to confirm the accuracy of measurements. However these results show that there is no significant difference between the two results in terms of mean values. These data show that the standard deviations are about 20 - 30% of the mean values both for Newtonian flows and dilute polymer flows and a little smaller than the standard deviations of the mean spacing of the streaky sturcture (30-40%) reported by Kline et al. (1967). Though these standard deviations should be taken into account in order to evuluate the mean values, these counts show that a reproducible average length scale of pocket pattern exists. While there is certainly some subjectiveness in the counting procedure, visual counts by different observers were in sufficient agreement as to be clearly meaningful. The results by different observers for Runs 2 and 3 are presented in figure 3.4 (symbol X). We estimate that the difference between differeant observers is no more than 20%.

Figure 3.4 shows that the length scale of pockets for the dilute polymer flows are bigger than those for the Newtonian flows. This was expected from the effect of dilute polymer on streaky spacing which is closely related to the pockets. The length scale of pockets for the dilute polymer flows averages about 87 wall layer units while the average length scale of pockets for the Newtonian flows is about 65, when averages are calculated over the range of the Reynolds numbers covered in the experiments. The increase in the length scales is about 30%, on average, and is smaller than the streaky spacing increase of 50-70%, for the same amount of drag reduction, observed by Oldaker and Tiederman (1977) as shown in figure 3.4. That is, the streaky spacing increases from about $\bar{\lambda}^+ = 100$ to about $\bar{\lambda}^+ = 160$. This means that pockets are less sensitive than the streak spacing in terms of structural changes by addition of polymer in channel flows. As mentioned in Chapter 2, a different criteria for the width of pockets is possible to adopt. The results obtained by a different criteria of (W) are given in Appendix F.

We can not infer the Reynolds number dependence of the length scale of pockets in the channel flows, because of the narrow range of Reynolds numbers covered in the experiments.

Time scales of pocket pattern obtained from the Newtonian flow and the dilute polymer are presented in figure 3.6. As discussed for the length scale of pockets, these counts of time between bursts also show that a reproducible time scale of the pocket pattern can be measured. Difficulties in counting arise because of ambiguities in determening exactly when a pocket started to form (Stage I) and when it has decayed beyond Stage V. Although there is more room for subjectiveness in the visual counts of time between pockets obtained by different observers compared to the measurement of the pocket widths, visual counts by different observers were in sufficient agreement as to be apparently meaningful. Corraborating results by different observers for Runs 2 and 3 are given in figure 3.6 (symbol X). We estimate that the difference of counts between different observers is no more than 30%.

Histograms of the time scale counting for both the Newtonian flows and dilute polymer flow are presented in figure 3.7. These data show that the standard deviations are about 60-80% of the mean values for the Newtonian flows and about 80-90% for the dilute polymer flows. The addition of dilute polymer to channel flows does not significantly affect the standard deviations of the time scale of pockets.

A striking result is obtained from this figure. The average time scale of pockets for the dilute polymer flows is 2.7 times, an average, as long as those for the Newtonian flows when averages are calculated over our range of the Reynolds number. The effects of a dilute polymer is more apparent on the time scale than on the length scale. This result indicates that dilute polymer solutions inhibit the occurrence of pockets substantially. Since the formation and break-up of pockets is known to be a main source of the turbulence production, the change in the frequency of occurance of pockets in the dilute polymer flows gives striking evidence that pockets are the footprint of the major turbulence production mechanism, which produces the flow drag. In other words, the drag reduction resulting from addition of a polymer is associated with the lower frequency of occurrence of the dominant eddies each of which contributes to the turbulence production. Data of time scales ($\bar{T}_*^+$) and ($\bar{T}_*'$) which are based on the wall layer coordinates and the outer layer coordinates respectively show a similar tendency along the Reynolds number axis. This result indicates that both the inner region flow and the outer region flow contribute to the formation of pockets.

It should be noted that the time scales ($\bar{T}_*^+$) and ($\bar{T}_*'$) seem to be dependent on the Reynolds number both for the Newtonian flows and the dilute polymer flows. This matter is left for discussion in Chapter 4.

CHAPTER 4

DISCUSSION

Available information about the effect of a dilute polymer on sublayer structure is given by Oldaker and Tiederman (1977) and Donohue et al. (1972). They suggested that the mechanism by which a dilute polymer solution achieves drag reduction is by inhibiting the formation of streaks. Their experimental results show that the average time between the bursts of an individual streak in the drag-reducing solutions is at the level expected for a Newtonian flow at the reduced wall shear. This result is presented in figure 4.1 and compared with the present data. Their result means that a decrese in production of turbulence results only from an increse in streak spacing because there is little change in the burst rate ($\bar{T}_B$) . However, the present data reveal an apparent difference of ($\bar{T}_B$) between the Newtonian flows and the dilute polymer flows at the same wall shear velocity. Donohue et al. (1972) also implied that the non-dimensional time between bursts was essentially constant (see Appendix G) where their data is plotted. The present data also show an important difference in the non-dimensional time between bursts ($\bar{T}_B^+$) between the

Newtonian flows and the dilute polymer flows. Hence, the present result provides a different story for the mechanism of drag reduction by a dilute polymer solution. That is, a dilute polymer solution affects both the length scale and the time scale of pockets independently. As mentioned in Chapter 3, the drag reduction resulting from addition of a polymer in channel flow is associated with the lower frequency of occurrence of pockets.

Donohue's counting technique was largely responsible for his misleading conclusions. He measured the streaky spacing, and counted the spatially averaged bursting rate $\bar{F}$ (bursts/m.sec.), where $\bar{T}_B = 1/(\bar{F} \cdot \bar{\lambda})$. The multiplication $\bar{F}$ and $\bar{\lambda}$ each of which vary in opposite directions, tended to leave the results unchanged from the Newton values. Hence, the direct counting of (T_B) employed in this present experiment, is necessary to separate the length and time scale changes.

The relationship between the streaky structure and the pocket pattern remains unclear. In this present observation, the streaky structure seems to be formed along with the evolution of pockets. The pockets are observable just downstream of the dye slit while the streaky structure is seen clearly downstream of the spots where the pockets are observed. As mentioned in Chapter 3, the length scale of pockets are less sensitive than the streaky spacing to the effects of addition of a polymer on the turbulence structure near the wall. This result means that the disappearance of pockets between streaks when polymers are added to newtonian flows brings much larger change of the the streaky spacing than change of the length scale of pockets themselves.

As mentioned in Chapter 3, the time scale of pockets seems to be dependent on the Reynolds number. Since a pressure gradient is a function of the Reynolds number in channel flows, this Reynolds number dependence implies a pressure gradient dependence of the time scale of pockets. In table 4.1 calculated parameters associated with the effects of a pressure gradient are given. The non-dimensional pressure gradient parameter (K) and the non-dimentional shear stress gradient (Δ_T) are defined by Kline (1967) and Patel (1968) , respectively (Appendix H). Figure 4.2 and 4.3 are presented for comparison of the scales of pockets between the present data and the results from the boundary layer flows without pressure gradient given by Falco and Lovett (1981). Two points are noteworthy to mention about the effects of a pressure gradient.

First, these figures show that there are apparent deviations of the turbulence structures in the channel flow from the boundary layer flow without pressure gradient though the latter result is necessary to extrapolate into the same range of the Reynolds number. The length scale of pockets for the channel flow is bigger than that for the boundary layer flow without pressure gradient while the frequency of occurrence of pockets decreases when a pressure gradient stands.

Kline et al. (1967) revealed that there was a considerable effect of pressure gradient on the break-up in the streaky structure. As shown in figure 4.4 with the present data, there were less break-ups for favourable pressure gradients (K>0) and more break-ups for unfavourable ones (K<0). The present results are conistent with his results. This consludes that the change of the time scale of pockets associated with the Reynolds number is an effect of pressure gradient in channel flow.

There is the different source of energy for the turbulence production process between the two type of flows. In the channel flow, a portion of the flow work produced by pressure gradient is converted to turbulence energy while in the boundary layer, the mean kinetic energy is used in the turbulence production process. However, to determine the mechanism of turbulence production near the wall under pressure gradient, extensive study of the outer region flow would be required.

Second, the present results of the time scale of pockets for the Newtonian flow show an increase in the time scale associated with the decrease in the Reynolds number and the non-dimentional shear stress gradient shown in table 4.1. This result is consistent with the reversion procedure of turbulent to laminar flow discussed by Patel and Head (1968). According to their data the reversion of turbulent to laminar flow occurs at $\Delta_\tau \leq -0.009$. The present results show that the experiments had been done in the turbulence region. Finally, it should be mentioned that by counting the length scale and the time scale of pockets for the boundary layer flow the author confirmed no significant difference associated with the data reduction process between the present ones and those employed by Falco and Lovett (to be published). Symbol (□) shows the results of the boundary layer flows done by the author.

Chapter 5

CONCLUSIONS

Addition of small concentrations of a polymer molecule to a Newtonian flow is shown to affect both the length scale and the frequency of occurrence of the turbulence production mechanism near a wall. We have shown that the length scale has increased about 30% and the frequency of occurrence of pockets has, over the range of the Reynolds number of 10,000 to 20,000, halved for 100 wppm concentration of Separan AP273 in which drag has been reduced about 40%. Thus, we have established that the drag reduction found in a dilute polymer is largely a result of the lower frequency of occurrence of pockets each of which contributes to the turbulence production.

The existance of a pressure gradient in a channel flow is shown to change both the length scale and the time scale of turbulence production mechanism near the wall. We have shown that a favourable pressure gradient in a channel flow has increased the length scale and has decreased the frequency of occurrence of pockets when compared to those scales of boundary layer flow without pressure gradient. However, the mechanism of the effects of a pressure gradient in a channel flow remains unknown.

Extensive investigations of the changes in outer flow structure associated with the turbulence production mechanism is necessary to help understand why their is such a large decrease in the pocket frequency and an increase in its scale.

APPENDIX A

Momentum thickness in channel flow

The Reynolds number (Re_θ) which is based on momentum thickness (θ) and centerline velocity (V_c) in a fully-developed and two-dimensional channel flow is derived as follows.

Steady incompressible and fully-developed flow is assumed. The velocity profile of a power-law form can be used.

$$u = A \cdot y^{1/n} \tag{1}$$

Where A is constant and 1/n is power.

Then, the momentum thickness (θ) becomes

$$\theta = \int_0^\delta u/V_c(1 - u/V_c)dy \tag{2}$$

where (δ) is the boundary layer thickness.

Since the dominant boundary layers in a two-dimensional channel are the ones which develop on the top and bottom surface. The boundary layer thickness can be set equal to (h/2).

Then the centerline velocity becomes,

$$V_c = A \cdot \delta^{1/n} = A \cdot (h/2)^{1/n} \tag{3}$$

Substitution of equations (1) and (3) into equation (2) and integration gives:

$$\theta = nh/\{2\cdot(n+1)(n+2) \qquad (4)$$

The centerline velocity in terms of the mean velocity (V_m) can be obtained as follows.

Since the channel is two-dimensional, becomes

$$V_m = \left(\int_0^{h/2} u\, dy\right)/(h/2) \qquad (5)$$

Substitution of equation (1) in equation (5) and integration yields

$$V_m = A\cdot n\,(h/2)^{(n+1)/n}/\{(h/2)(n+1)\} \qquad (6)$$

Then, equation (6) can be arranged by equation (3).

$$V_m = A\cdot n\,(h/2)^{1/n}/(n+1) = n\,V_c\,/\,(n+1) \qquad (7)$$

Therefore, the Reynolds number($R_{e\Theta}$) can be obtained in terms of the mean velocity (V_c) and the hydraulic diameter (D_h).

Then

$$R_{e\Theta} = R_e D_h/\{4(n+2)\} \qquad (8)$$

where

$$Re_{D_h} \equiv V_m \cdot D_h / \nu = V_m \cdot (2h) / \nu$$

(Re_{D_h}) is based on hydraulic diameter (D_h) and mean velocity (V_m).

As an estimate of power (n), n=7 was used because the power law velocity profile with the number 7 is a quite good fit for pipe flows for moderate Reynolds numbers.

*Kays, M.W. and Crawford, E.M. 1980. Convective heat and mass transfer Second edition, McGraw-Hill series in Mechanical Engineering.

APPENDIX B

Derivation of friction coefficient

The friction coefficient f is defined as follows:

$$f = 4\tau_w / (\rho \cdot V_m^2 / 2) \qquad (1)$$

where

(τ_w) is wall shear stress and (V_m) is mean velocity of channel.

(τ_w) is obtained from pressure gradient (dp/dx). That is, under the assumption of fully-developed channel flows, the momentum balance for the control volume gives

$$0 = \{p - (p+\Delta p)\} h \cdot b - 2(h+b) \cdot \tau_w \cdot \Delta x$$

As $\Delta x \rightarrow 0$, the momentum equation yields

$$\tau_w = -(dp/dx) \cdot b \cdot h / \{2(h+b)\}$$

or

$$\tau_w = -(dp/dx) \cdot Dh / 4 \qquad (2)$$

where $Dh\,(=4bh/\{2(h+b)\})$ is the hyraulic diameter of channel.

Combination of equations (1) and (2) yields

$$f = -(dp/dx) \cdot Dh / \{\rho V_m^2 / 2\} \qquad (3)$$

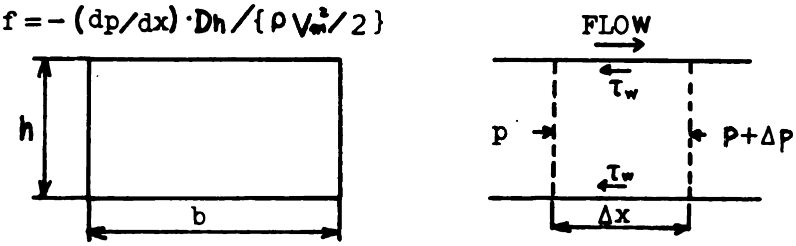

Figure(B) Momentum balance

APPENDIX C

Injection rate of dye

M is defined as the relative amount of dyed fluid in the sublayer. That is, the ratio of the dyed flow rate to the flow rate in the sublayer passing over the dye slit.

Thickness of the viscous sublayer is assumed to be?r equal to $y^+ (= y u_\tau / \nu) = 8$ because Reischman * (1975) have shown that the non-dimensional thickness of the sublayer is essentially the same both for Newtonian and drag-reducing flows. Hence, the operational relationship for M is

$$M = \dot{Q}_d / \left(b \int_0^{8\nu/u_\tau} u \, dy \right) \qquad (1)$$

where is the flow rate of dyed fluid, and b is the spanwise length of the dye slit. In the viscous sublayer, u is given by

$$u = y \cdot u_\tau^2 / \nu \qquad (2)$$

Substitution of equation (2) into equation (1) yields

$$M = \dot{Q}d / (32 b \nu) \qquad (3)$$

* Reischman, M. M. and Tiederman G. W. 1975 Laser-Doppler anemometer measurements in drag-reducing channel flows J. Fluid Mech. 70 p 369.

APPENDIX D

Material properties of Separan AP273

Separan AP273 synthetic polymer is a high-molecular-weight, water-soluble, anionic polyacrylamide.

(1) Typical Properties

Ionic Character	Anionic
Physical Form	White granular
Bulk Density	47lbs./cu. ft.
Residual Monomer Content	0.3%
pH (0.5% solution, 68 F/20 C)	10.1
Particle size (NO. 35 mesh, U.S. Standard Sieve, minimum)	95%
Maximum Recommended Solution Strength	0.5%

(2) Recommended storage conditions

Length of Storage:

Stock solution (0.5%)	1 month
Laboratory Solution (0.1%)	1 day

Temperature

Dry product	<100 °F (38 °C)
Solutions	<120 °F (48 °C)

(3) Corrosivity

Solutions are essentially noncorrosive and standard materials of construction can be used for all equipment. Zinc, aluminum and magnesium are exceptions. Therefore, galvanized equipment should not be used. Black iron and mild steel have been used satisfactorily for handling anionic solutions. Preferred materials of construction are stainless steel and corrosion-resistent plastic.

(4) Solution makeup.

Because of the high molecular weight of Separan AP273 stock solutions are usually limited to 0.5% or less. Higher concentrations present handling problems because of their high viscosity. As with other Separan polymers, good dispersion is essential and best accomplished with a Dow-approved disperser. Transfer pumps should be either gear or positive-displacement piston pumps.

(5) Note on Viscosity data

Solution of Separan polymers often exhibit non-Newtonian characteristics; solution viscosities are affected by shear. As shear stress increases, viscosities decrease. Figure (D) shows the viscosity of Separan AP273.

The above information is from citation of the catalog for AP273 by the Dow Chemical Company.

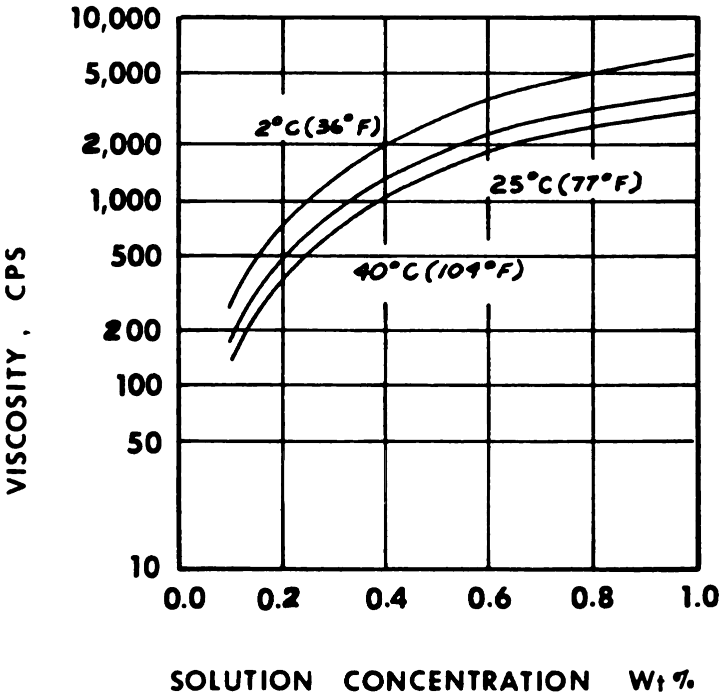

FIGURE (D) **VISCOSITY DATA FOR SEPARAN AP273**
(RVT Brookfield Viscometer, No. 5 Spindle, 20 RPM, from DOW CHEM. CO.)

APPENDIX E

Estimation of measurement accuracy

The overall accuracy of $(\overline{T}_B^+)$ and $(\overline{W}^+)$ are obtained as follows

$$\overline{T}_B^+ = \overline{T}_B \cdot u_\tau^2 / \nu \quad , \quad \overline{W}^+ = \overline{W} \cdot u_\tau / \nu \quad , \quad Re_{Dh} = Dh \cdot V_m / \nu \qquad (1)$$

Since,

$$u_\tau = \sqrt{\tau_w/\rho} = \sqrt{-(dp/dx) \cdot Dh/(4\rho)} \qquad (2)$$

$$\overline{T}_B^+ = -(dp/dx) \cdot \overline{T}_B \cdot Dh/(4\rho\nu) \qquad (3)$$

and

$$\overline{W}^+ = \overline{W}\sqrt{-(dp/dx) \cdot Dh/(4\rho)}/\nu \qquad (4)$$

Then the total differentials for T ,W and ReDh are

$$d\overline{T}_B^+/\overline{T}_B^+ = -d\nu/\nu + d\overline{T}_B/\overline{T}_B + d(dp/dx)/(dp/dx) \qquad (5)$$

$$d\overline{W}^+/\overline{W}^+ = -d\nu/\nu + d\overline{W}/\overline{W} + d(dp/dx)/\{2(dp/dx)\} \qquad (6)$$

and

$$dRe_{Dh}/Re_{Dh} = -d\nu/\nu + dV_m/V_m \qquad (7)$$

where both (ρ) and (Dh) are assumed to be constant. Finally, the error estimation given the by Gauss' equation of error propagation yields

$$(d\overline{T}_B^+/\overline{T}_B^+)_e = \{(d\nu/\nu)^2 + (d\overline{T}_B/\overline{T}_B)^2 + (d(dp/dx)/(dp/dx))^2\}^{1/2} \qquad (8)$$

$$(d\bar{W}^{+}/\bar{W})_e = \{(d\nu/\nu)^2 + (d\bar{W}/\bar{W})^2 + (d(dP/dX)/(2\cdot(dP/dX)))^2\}^{1/2} \quad (9)$$

and

$$(dRe_{Dh}/Re_{Dh})_e = \{(d\nu/\nu)^2 + (dV_\infty/V_\infty)^2\}^{1/2} \quad (10)$$

APPENDIX F

Criteria of pocket measurement

A number of criteria for the length scale of pockets are possible. For example, (W)can be measured by the spanwise length of pockets where dyed fluid is completely removed (named "Criteria B"). BThis criteria give a shorter length scale of pockets than the present one adopted by Falco and Lovett (named "Criteria A"). Figure (F) shows the length scale of pockets measured by criteria A. There is about 40% difference between the two criterias. As mentioned in Chapter 2, we have adopted Criteria B which is consistant with the criteria used in boundary layer measuments.

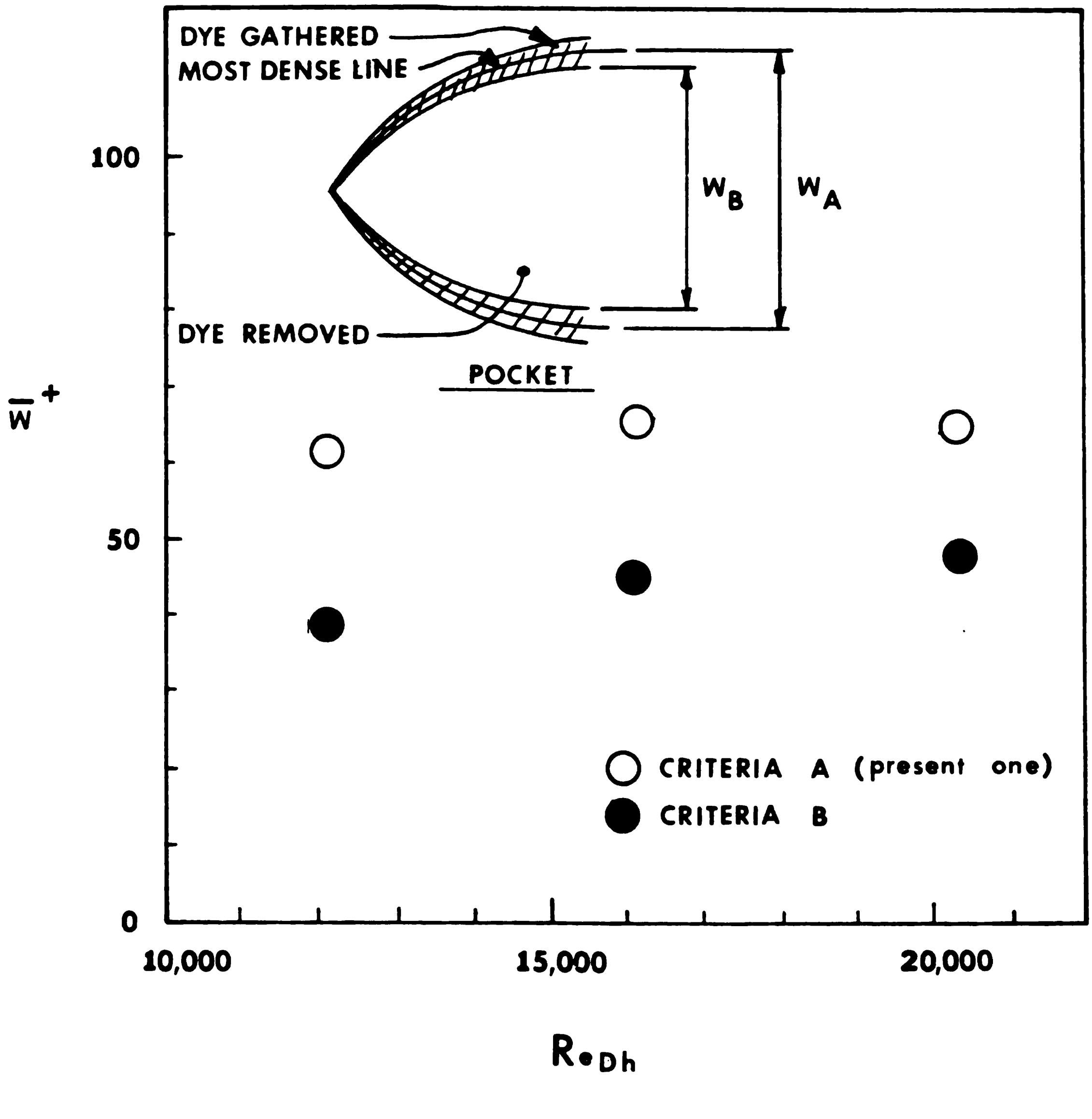

FIGURE (F) THE LENGTH SCALE OF POCKETS MEASURED BY A DIFFERENT CRITERIA

APPENDIX G

Donohue's results of time scale

Figure (G) shows Donohue's * (1972) results of $(\overline{T}_B^+)$ which are calculated from measurements of $\overline{F}$ and $\overline{\lambda}$. He indicated that the non-dimensional time between bursts is essentially constant. However, the present data which have much less scatter, show an apparent difference of $(\overline{T}_B^+)$ between Newtonain flow and dilute polymer flow.

* Donohue, L.G., Tiederman and Reischman, M.M. 1972 Flow visualization of the near-wall region in a drag-reducing channel flow J. Fluid Mech. 56, p. 559.

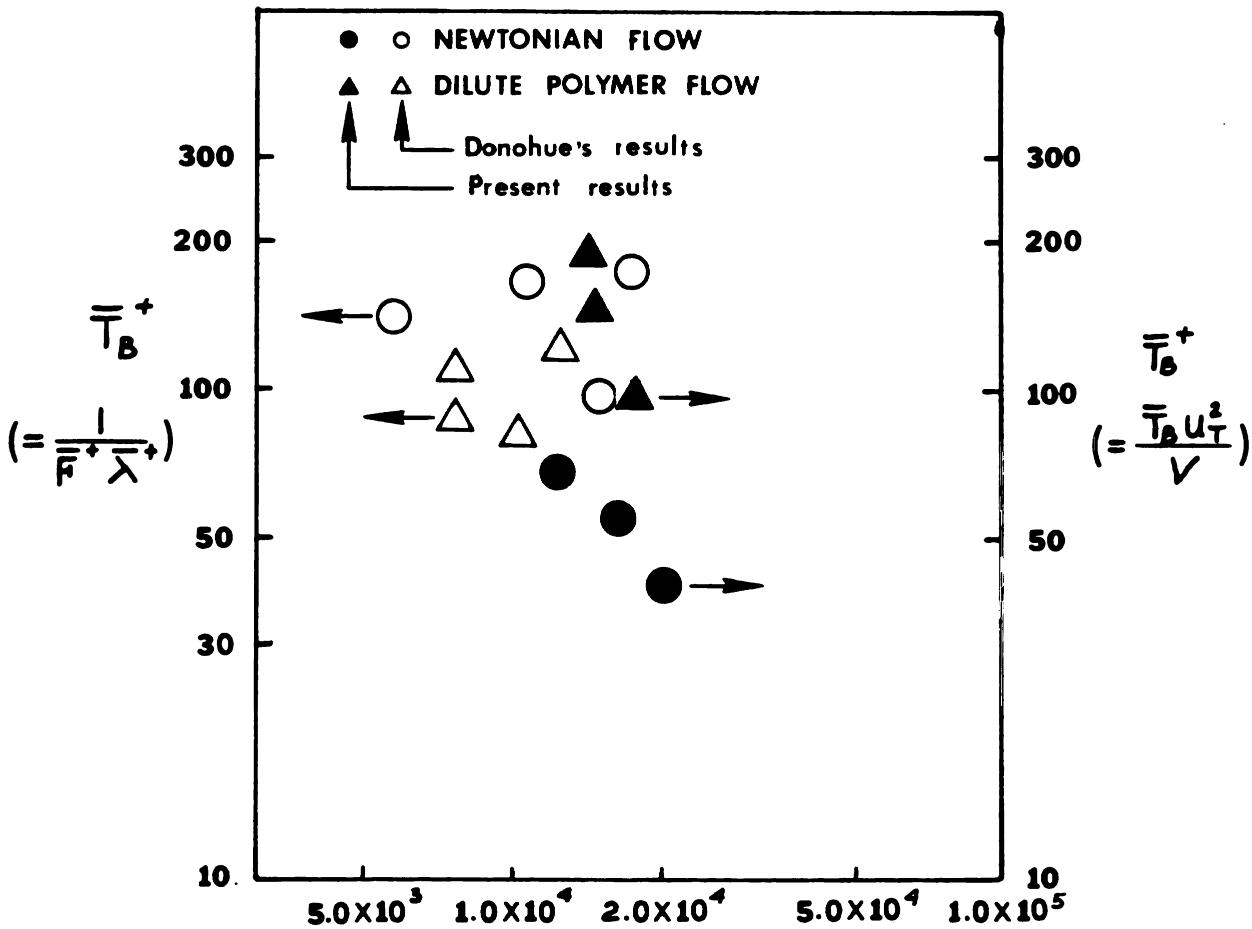

FIGURE (G) **COMPARISON BETWEEN DONOHUE'S AND PRESENT RESULTS**

APPENDIX H

Derivation of "α" for channel flow

The factor "α" for a channel flow is derived as follows:

"α" is defined as ($\tau = \tau_w + \alpha y$) by Townsend * (1962).

Momentum balance of the control volume shown in figure H gives

$$\tau \cdot dx\{2(b-2y)+2(h-2y)\} = -dp\cdot(b-2y)(h-2y) \qquad (1)$$

Rearrangement of the equation becomes

$$\tau = -(dp/dx)(b-2y)(h-2y)/\{2(b-2y)+2(h-2y)\} \qquad (2)$$

At y=0

$$\tau = \tau_w = -(dp/dx)\cdot bh/\{2(b+h)\} \qquad (3)$$

On the other hand, from the definition of "α"

$$\alpha = (\tau - \tau_w)/y \qquad (4)$$

Substitution of equations (2) and (3) into equation (4) yields

$$\alpha = (dp/dx)\{1-2b\cdot h/(b+h)^2\} \qquad (5)$$

Therefore the non-dimensional shear stress gradient Δ_τ ($=\alpha\cdot\nu/(\rho u_\tau^3)$) for a channel flow becomes

$$\Delta_\tau = (dp/dx)\{1-2b\cdot h/(b+h)^2\}\nu/(\rho u_\tau^3) \qquad (6)$$

because y is small enough to neglect the second order of y.

* Townsend, A.A., 1962 The behavier of a turbulent boundary layer near separation. J. Fluid Mech. 12 p536.

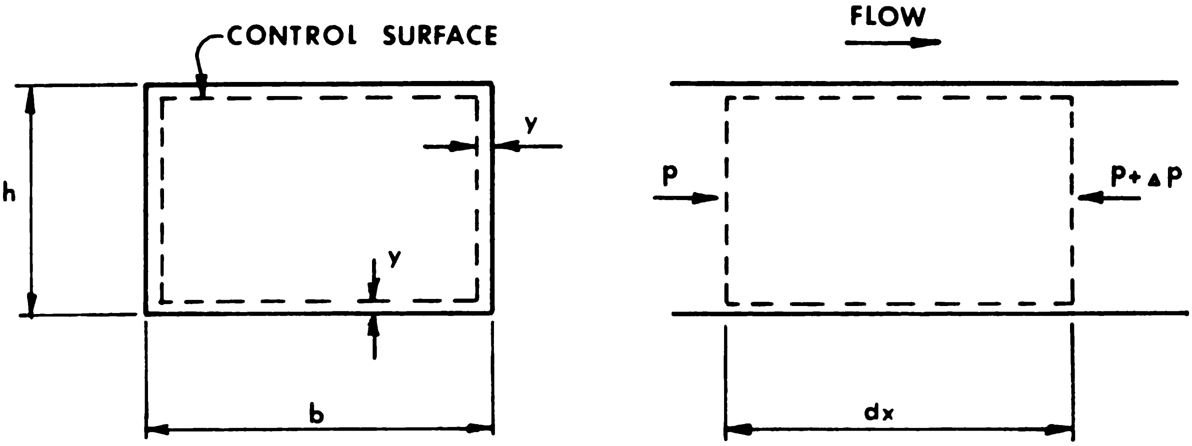

FIGURE (H) **MOMENTUM BALANCE OF CHANNEL FLOW**

REFERENCES

1. Bakewell, H.P. and Lumley, J. L. 1967
Viscous sublayer and adjacent wall region in turbulent pipe flow. Physics of Fluids 10, pp. 1880.

2. Donohue, G.L. et al. 1972. Flow visualization of the near wall region in a drag-reducing channel flow. J. Fluid Mech. 56, pp. 575.

3. Falco, R.E. 1977. A structural model of the turbulent boundary layer. Proceedings of the 14th annual meeting of the Society of Engineering Sciences.

4. Falco, R.E. 1980. The production of turbulence near a wall. AIAA 13th Fluid and Plasma dynamics conference, July, 1980.

5. Falco, R.E., and Wiggert, D.C. 1980. Effects of dilute polymer solutions on vortex ring/wall interactions. Viscous flow drag reduction, edited by G.R. Hough, 72 of Progress in Astronautics and Aeronautics.

6. Falco, R.E. and Lovett, J.A. The scaling of wall region structure. To be submitted to Phy Fluids

7. Hussain, F.M.K.A. and Reynolds, W.C. 1975. Measurements in fully developed turbulent flow. Fluid Mech. (Trans. ASME) December 1975, pp. 568-580.

8. Kays, M.W. and Crawford, E.M. Convective heat and mass transfer, 2nd edition. McGraw-Hill series in mechanical engineering.

9. Kline,S.J. 1978 The role of visualization in the study of the structure of the turbulent boundary layer. Coherent Structure of Turbulent Boundary layers,
ed. by C.R. Smith and D.E. Abbott, AFOSR/Lehigh.

10. Kline, S.J., Reynolds, W.C., Schranb, F.A., and Runstadler, P.W., 1967. The structure of turbulent boundary layers. J. Fluid Mech., 30 part 4, pp. 741-773.

11. Oldaker, D.K. and Tiederman, G.W. 1977. Spatial structure of the viscous sublayer in drag-reducing channel flows. Physics of Fluids, 20, p133.

12. Patel, V.C. and Head, R.M. 1968. Reversion of turbulent to laminar flow. J. Fluid Mech., 34, pp. 371-392.

13. Peterson, J.P. et al, 1973. High polymer drag reduction in open channel flow.

No. 130, vol. 69 AIChE Symposium Series, p82.

14. Reischman and Tiederman, G.W. 1975. Laser-Doppler anemometer measurements in drag-reducing channel flows. J. Fluid Mech., 70, pp. 369-392.

15. Tennekes, H. and Lumley, L.J. A first course in turbulence. Six printing 1980 MIT press.

16. Townsend, A.A. 1976. The structure of turbulent shear flows. Cambridge University Press. Cambridge, U.K.

17. Virk, S.P. 1975. Drag reduction fundamentals. AIChE J., pp. 625.

18. White, M.F. 1979. Fluid Mechanics, McGraw-Hill, Inc.

19. Willmarth, W.W. 1975 Structure of turbulence in boundary layers. Advances in Applied Mechanics, 15, Academic Press, N.Y.

TABLE 2-1 Accuracy of Measurements

		Accuracy (%)			Over-all accuracy (%)		
	Vm (m/sec)	Vm	dp/dx	ν	ReDh	$\overline{T}_B^+$	$\overline{W}^+$
Newtonian	0.2	2.5	5.0	2	3.2	5.4	3.2
flow	0.26	3.3	3.0	2	3.9	3.6	2.5
	0.4	4.0	1.2	2	4.5	2.3	2.1
Dilute	0.2	2.5	8.3*	5	5.6	9.7	6.5
polymer	0.26	3.3	5.0*	5	6.0	7.1	5.6
flow	0.4	4	2.0*	5	6.4	5.4	5.1

* based on 40% drag reduction

TABLE 3.1 SUMMARY OF EXPERIMENTS

Run	Solvent	Average Velocity V_m (M/S)	Wall Shear Velocity U_τ (M/S)	Drag Reduction (%)	Temperature t (°C)	Kinematic Viscosity ν (M^2/S)	ReDh	$\overline{W}$ (MM)	$\overline{T}_B$ (S)	$\overline{W}^+ = \frac{\overline{W} U_\tau}{\nu}$	$\overline{T}_B^+ = \frac{\overline{T}_B U_\tau^2}{\nu}$	$\overline{T}_B' = \frac{\overline{T}_B V_m}{(Dh/2)}$
1	water	0.225	0.0153	0	13	1.2×10^{-6}	12100	4.98	0.353	63.5	68.9	2.46
2	water	0.300	0.0190	0	13	1.2×10^{-6}	16100	4.19	0.181	66.3	54.5	1.68
3	water	0.380	0.0240	0	13	1.2×10^{-6}	20400	3.28	0.082	65.6	39.4	0.97
4	water +AP273 100wppm	0.331	0.0187	29(27)	27	1.49×10^{-6}	14300	6.78	0.832	85.1	195.	8.54
5	water +AP273 100wppm	0.345	0.0189	33(28)	27	1.49×10^{-6}	14900	6.79	0.617	86.1	148.	6.60
6	water +AP273 100wppm	0.400	0.0202	40(36)	27	1.49×10^{-6}	17300	6.67	0.362	90.4	99.1	4.48

( ) Based on the solvent Reynolds number

TABLE 4.1 Calculated Parameters

RUN	SOLVENT	ReDh	$R_{e\Theta}$*	$\Delta_T \equiv \alpha \frac{\nu}{\rho u_\tau^3}$	K $\equiv -\frac{\nu}{\rho V_c^3}\frac{dP}{dx}$	$-\frac{dP}{dx}$ (kg/m²)
1	WATER	12100	336	-0.0036	1.0×10^{-6}	1.48
2	WATER	16100	447	-0.0029	0.67×10^{-6}	2.28
3	WATER	20400	567	-0.0230	0.52×10^{-6}	3.64
4	SOL.**	14300	397	-0.0037	0.6×10^{-6}	2.21
5	SOL.**	14900	414	-0.0035	0.54×10^{-6}	2.26
6	SOL.**	17300	481	-0.0034	0.40×10^{-6}	2.58

* Appendix A

** Water + Ap273 100 wppm

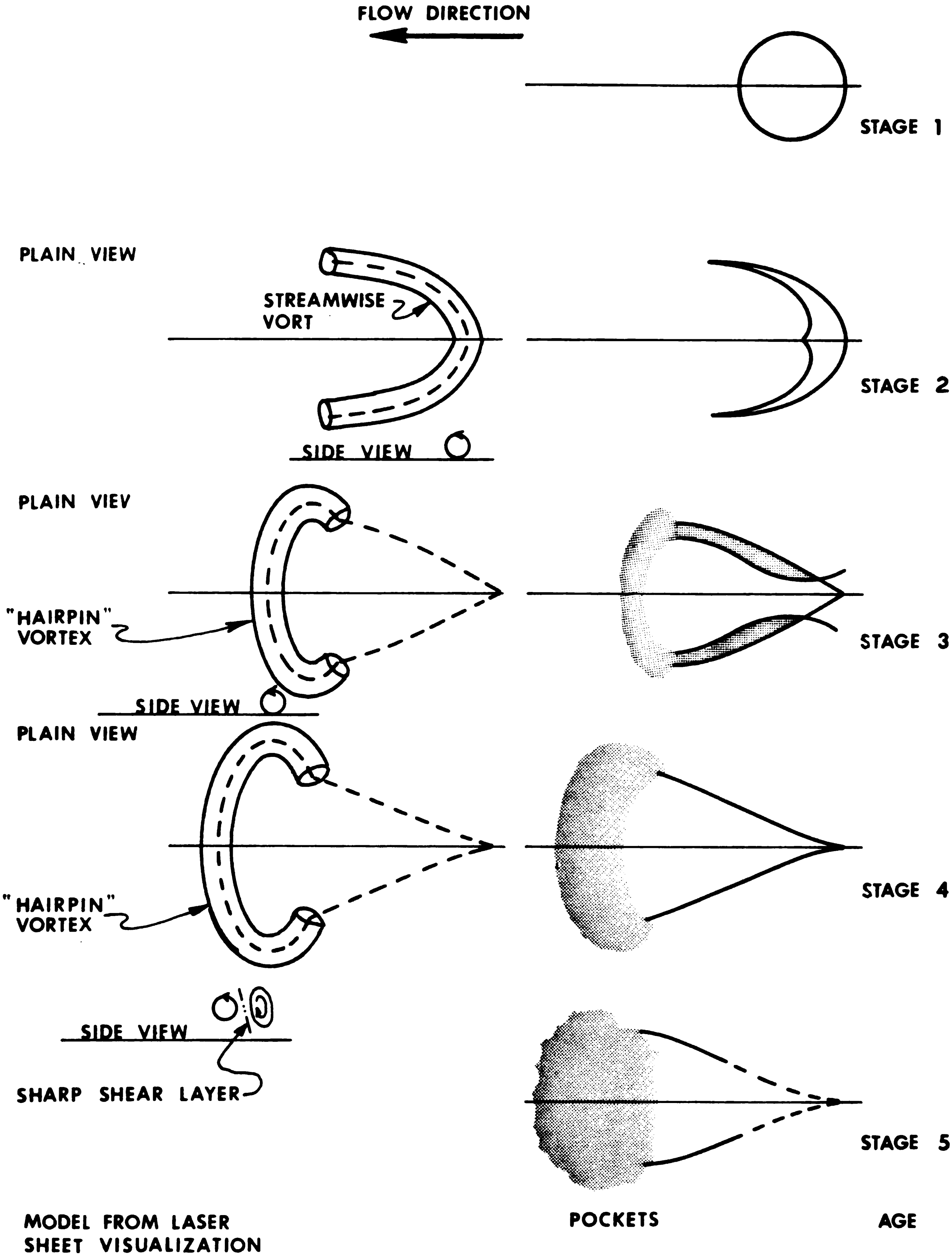

FIGURE 1.1 **SKETCHES OF THE EVOLUTION OF POCKETS**

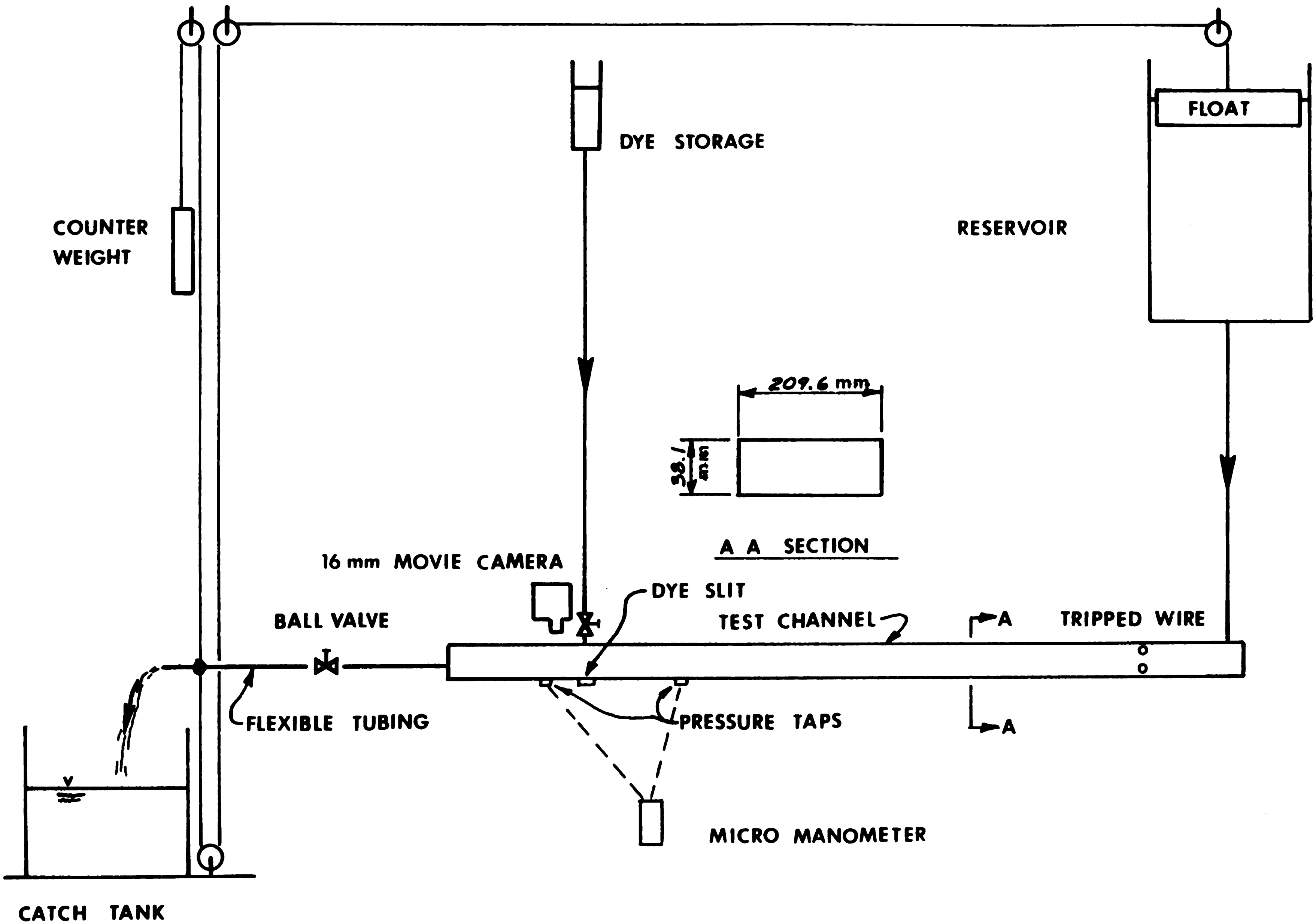

FIGURE 2.1 **FLOW SYSTEM OF TEST CHANNEL**

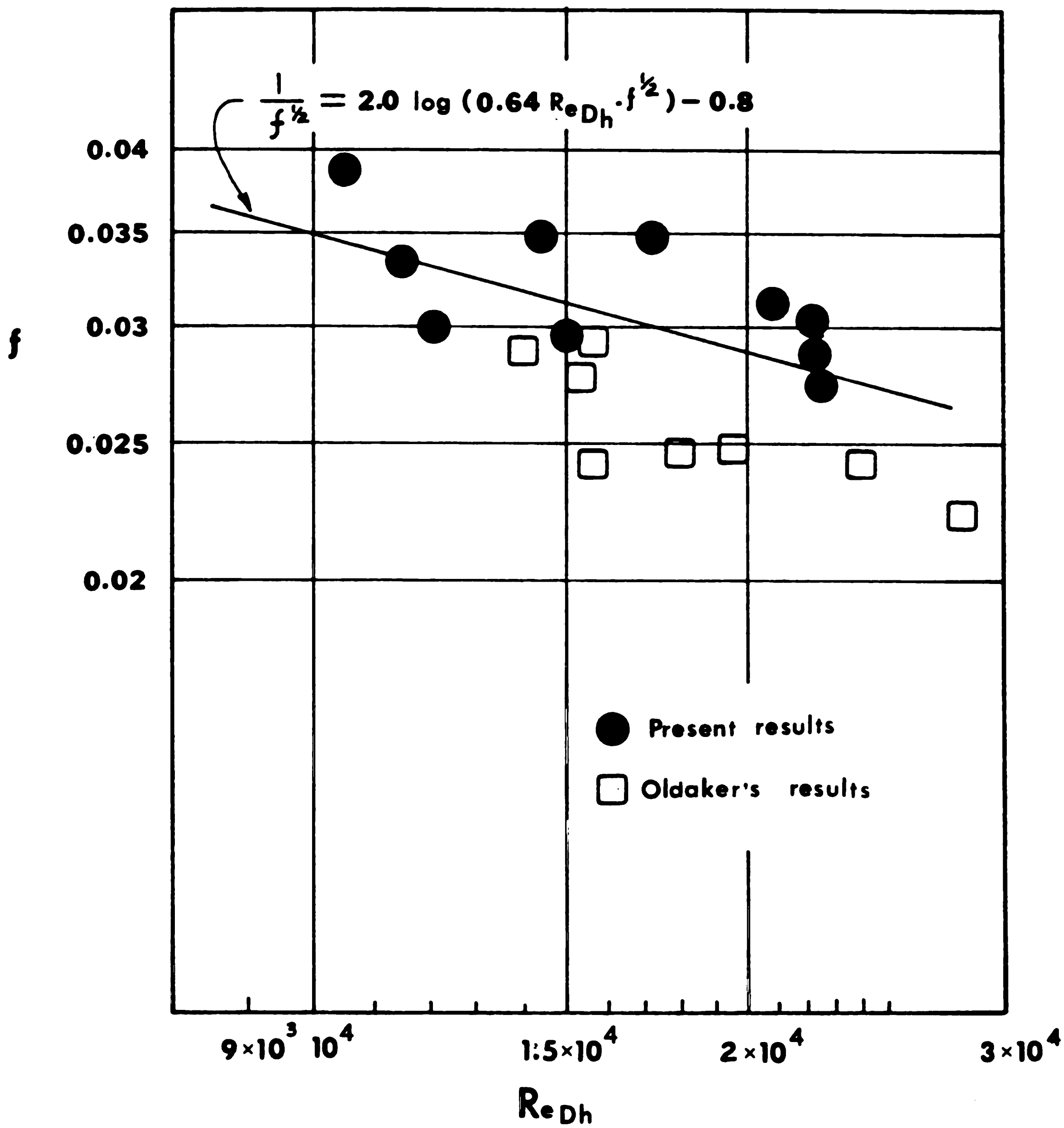

FIGURE 2.2 FRICTION COEFFICIENT OF CHANNEL FOR NEWTONIAN FLOW

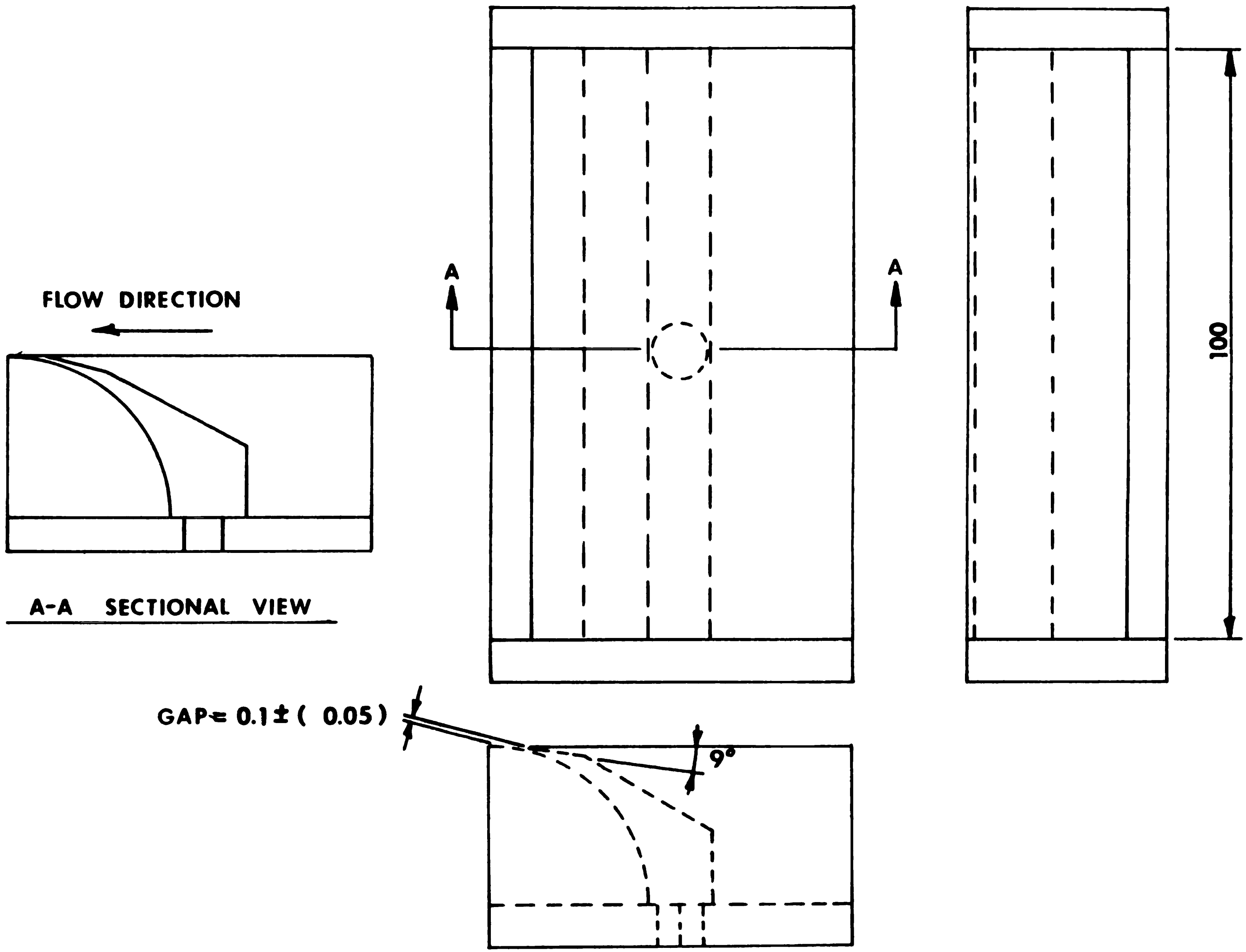

FIGURE 2.3 **DYE SLIT** unit (mm)

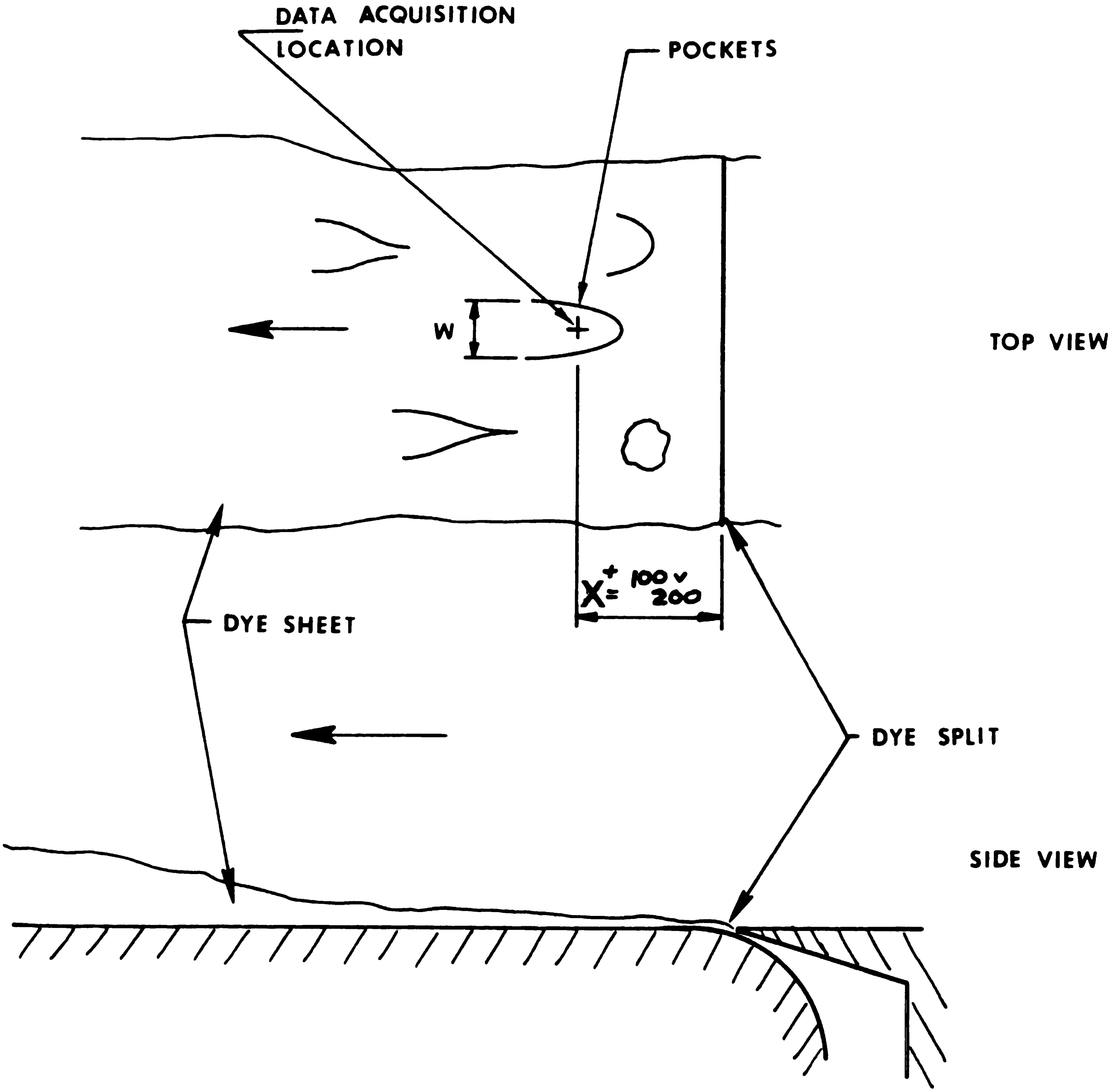

FIGURE 2.4 **METHOD OF POCKET COUNTING**

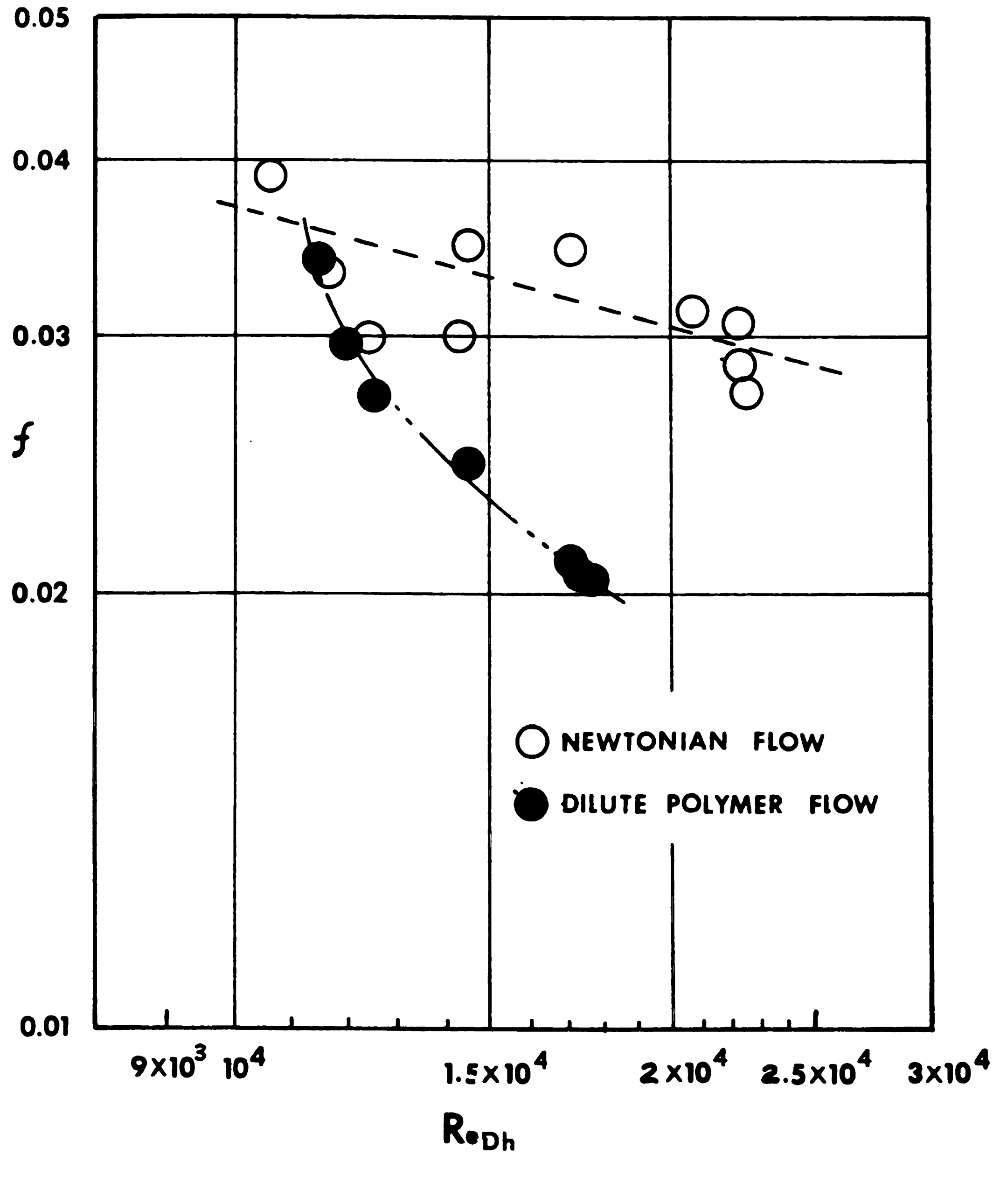

FIGURE 3.1 **FRICTION COEFFICIENT OF CHANNEL**

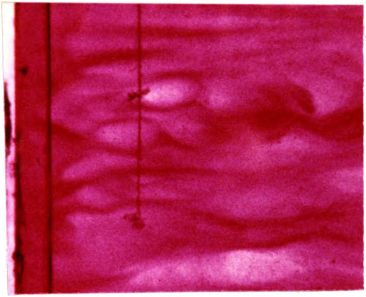

(a)

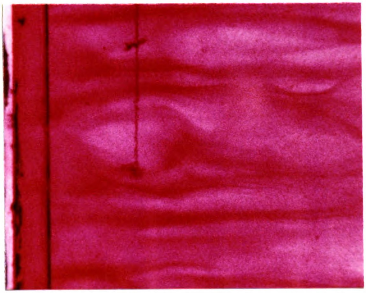

(b)

Figure 3.2 Dye slit visualization of the sublayer flow field in a channel, showing the pockets in water. Both photos are at Re_{Dh} = 16,100. Flow is from left to right.

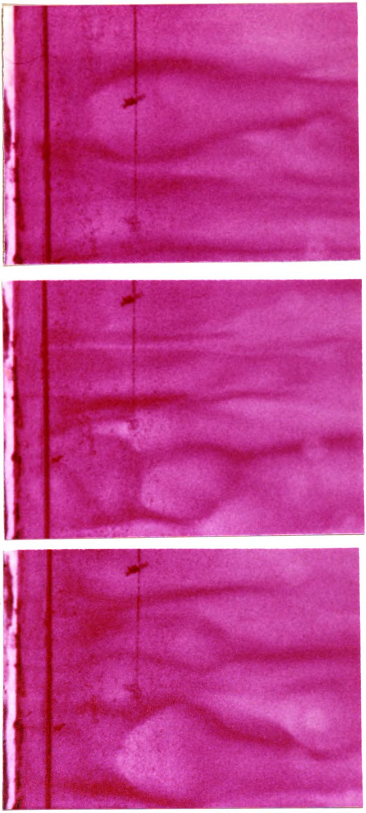

(a)

(b)

(c)

Figure 3.3 Visualized sublayer flow showing the pocket patterns in 100 ppm solution of Separan AP273. (a,b); Re_{Dh} = 14,300: (c); Re_{Dh} = 17,300. The flow is from left to right.

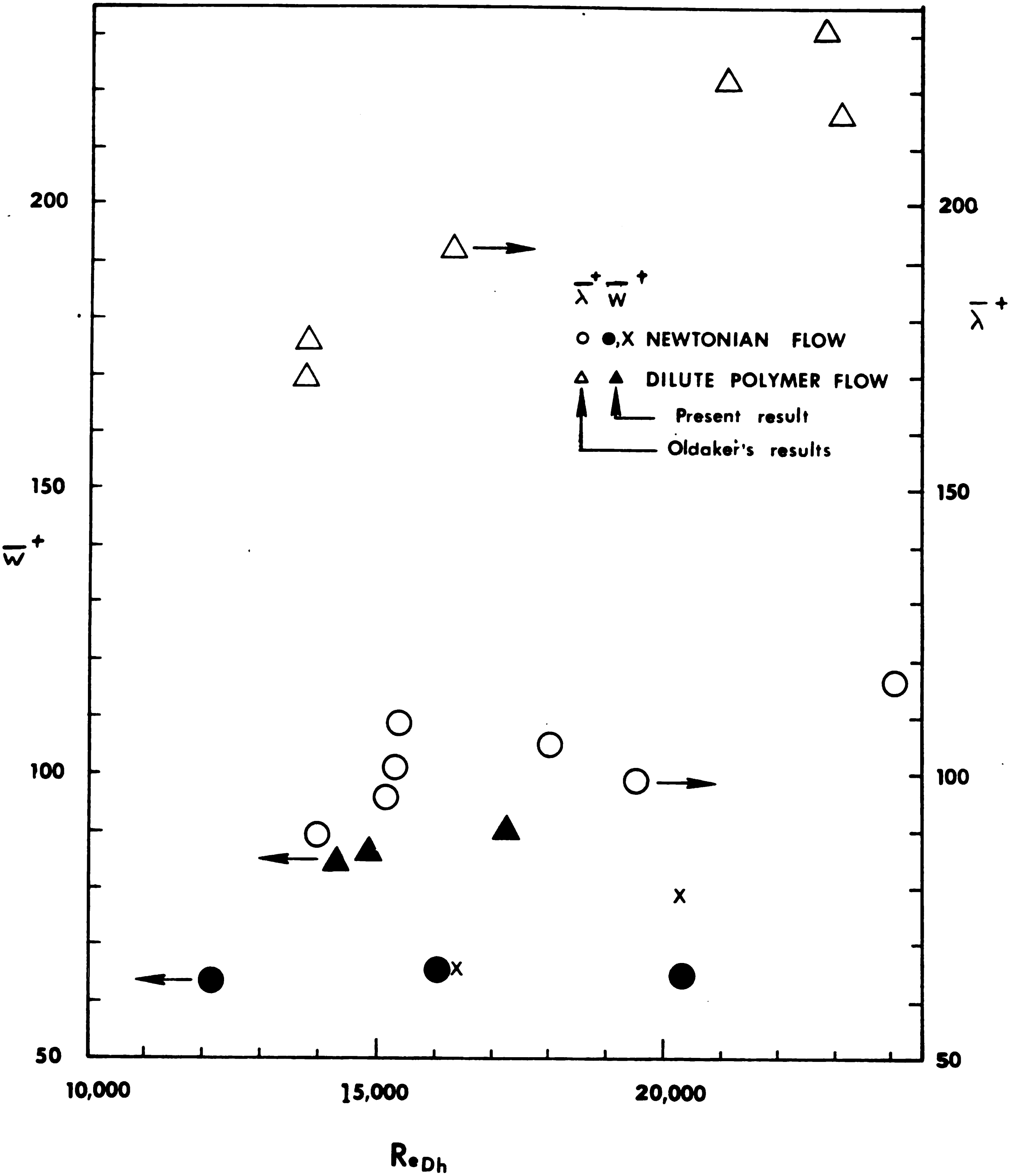

FIGURE 3.4 **LENGTH SCALE OF POCKETS**

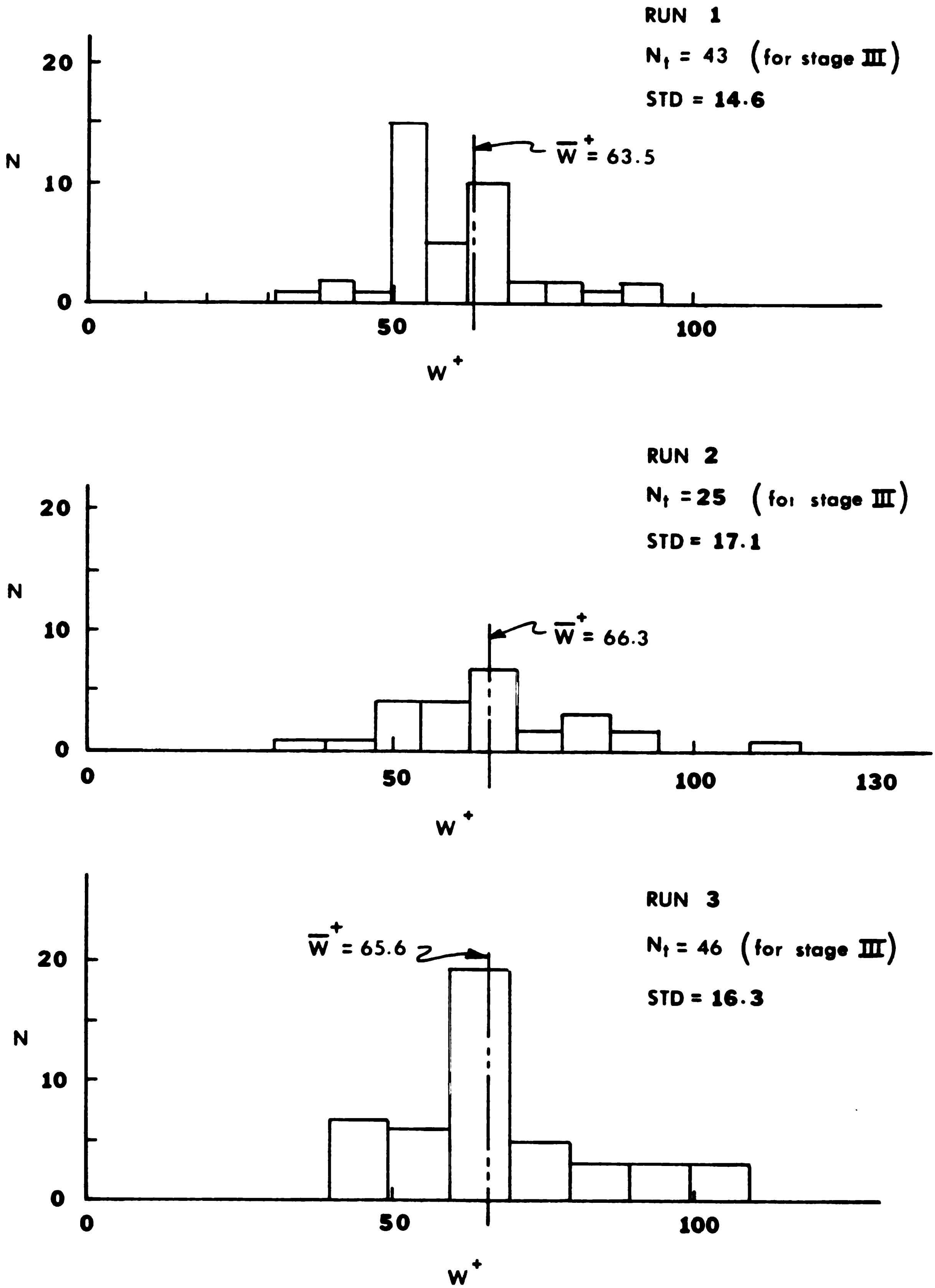

FIGURE 3.5 (A) HISTOGRAM OF LENGTH SCALE OF POCKETS

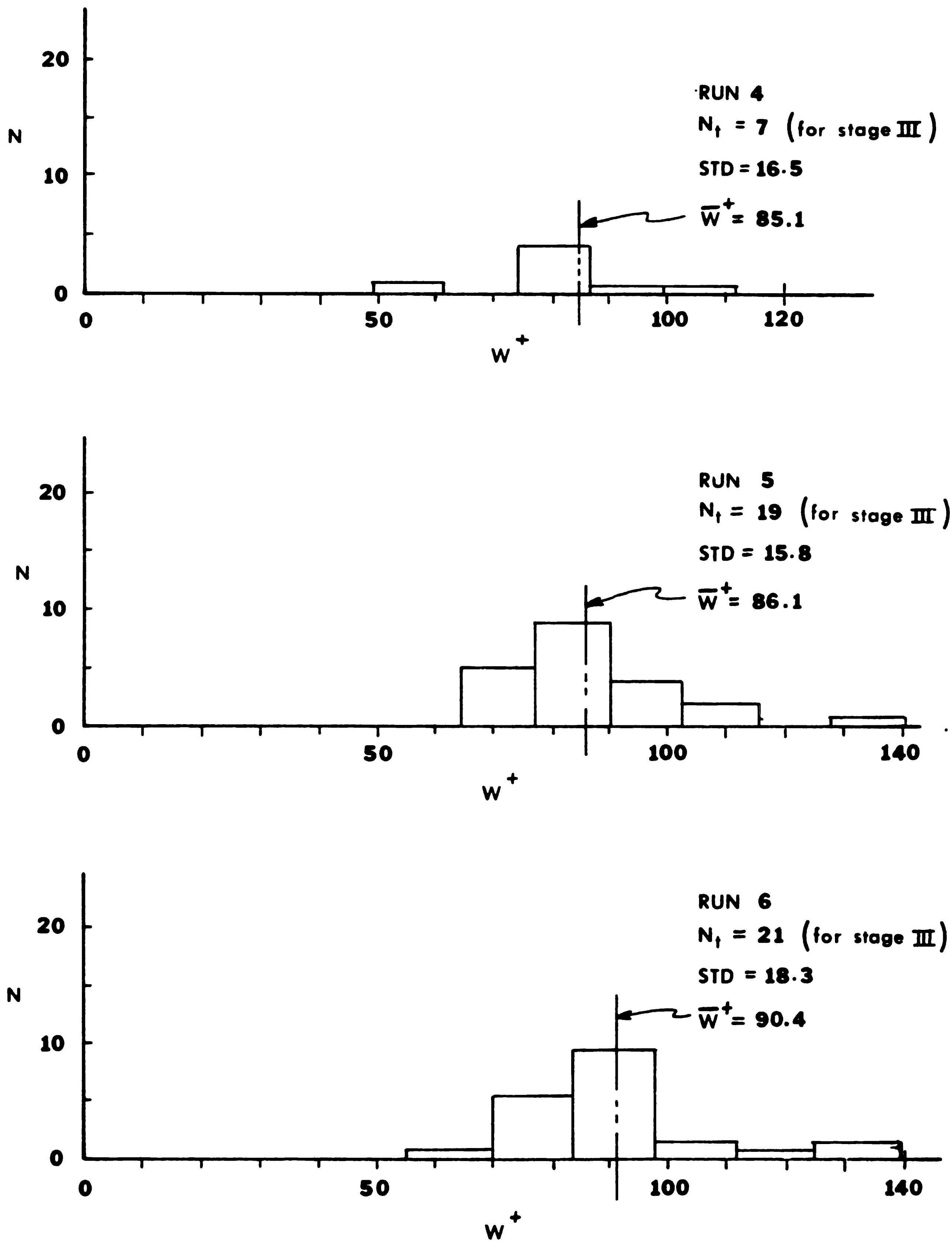

FIGURE 3.5(B) **HISTOGRAM OF LENGTH SCALE OF POCKETS**

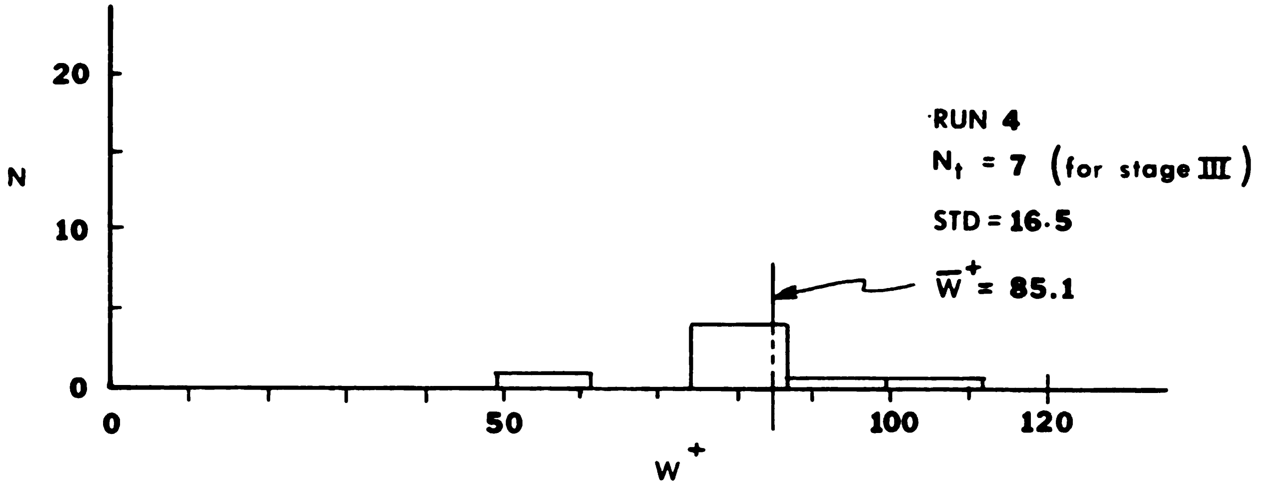

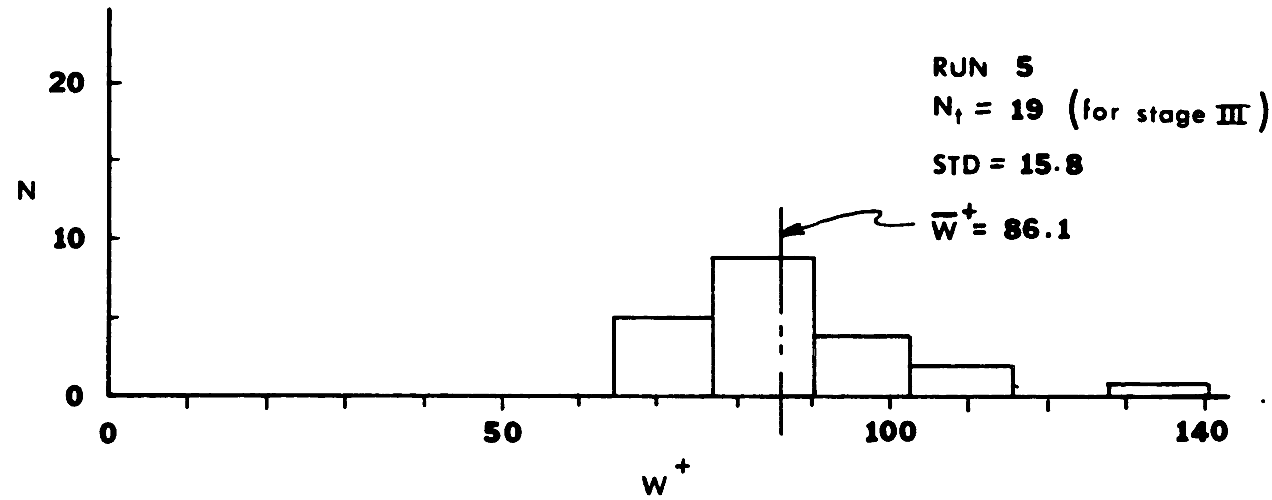

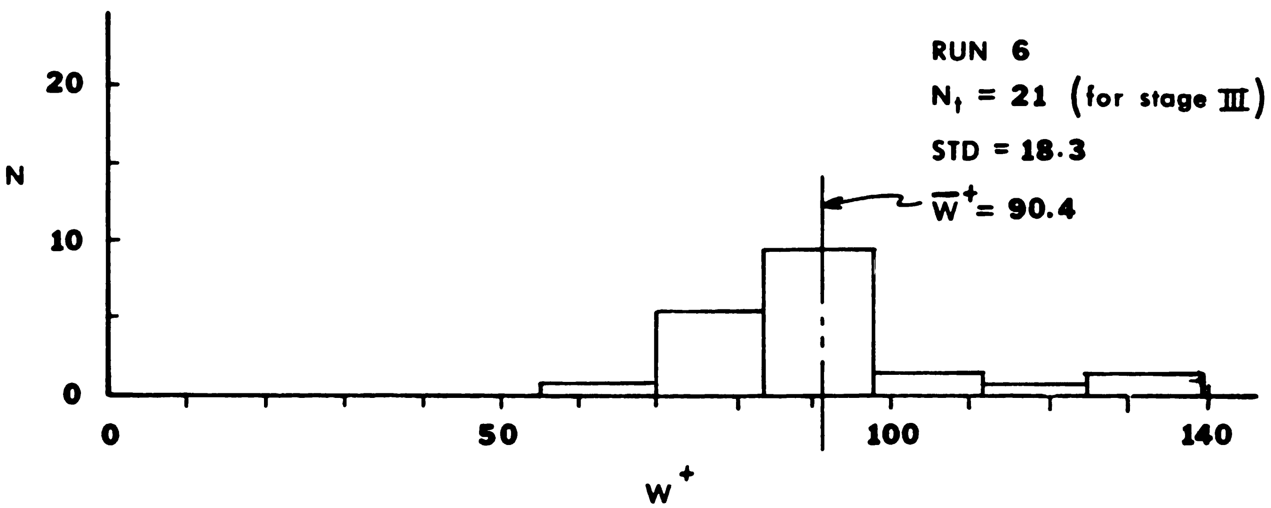

FIGURE 3.5(B) **HISTOGRAM OF LENGTH SCALE OF POCKETS**

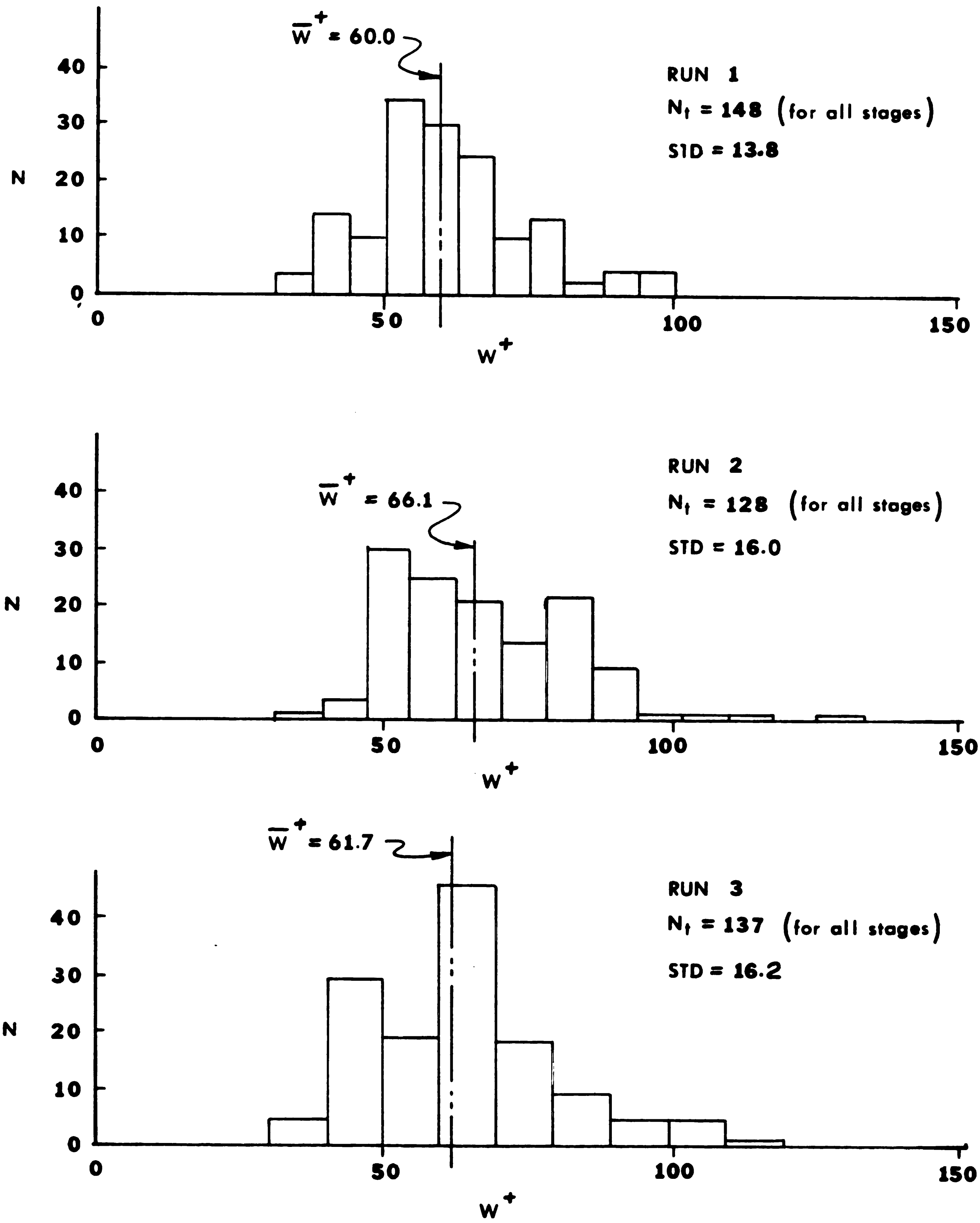

FIGURE 3.5 (C) **HISTOGRAM OF LENGTH SCALE OF POCKETS**

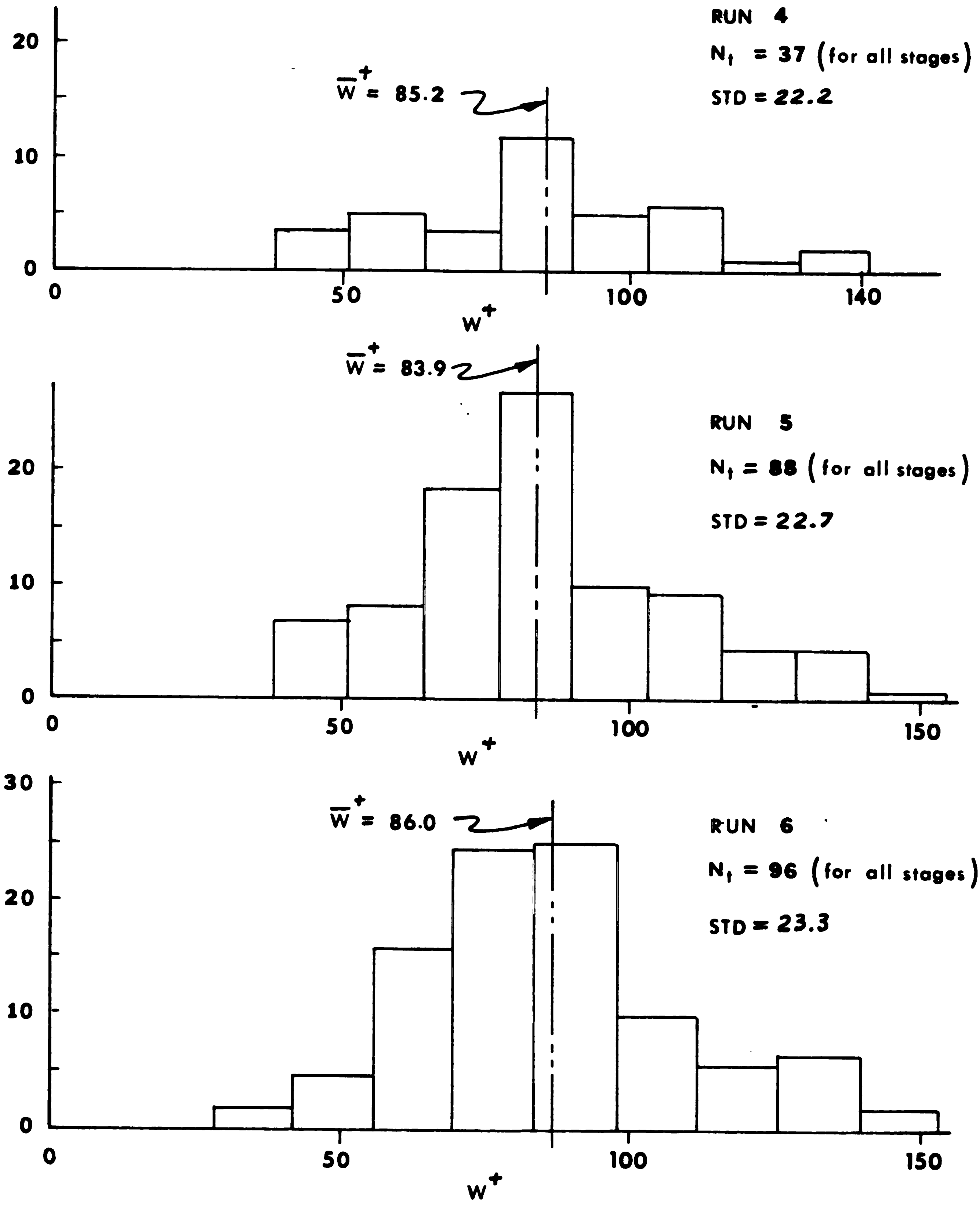

FIGURE 3.5(D) **HISTOGRAM OF LENGTH SCALE OF POCKETS**

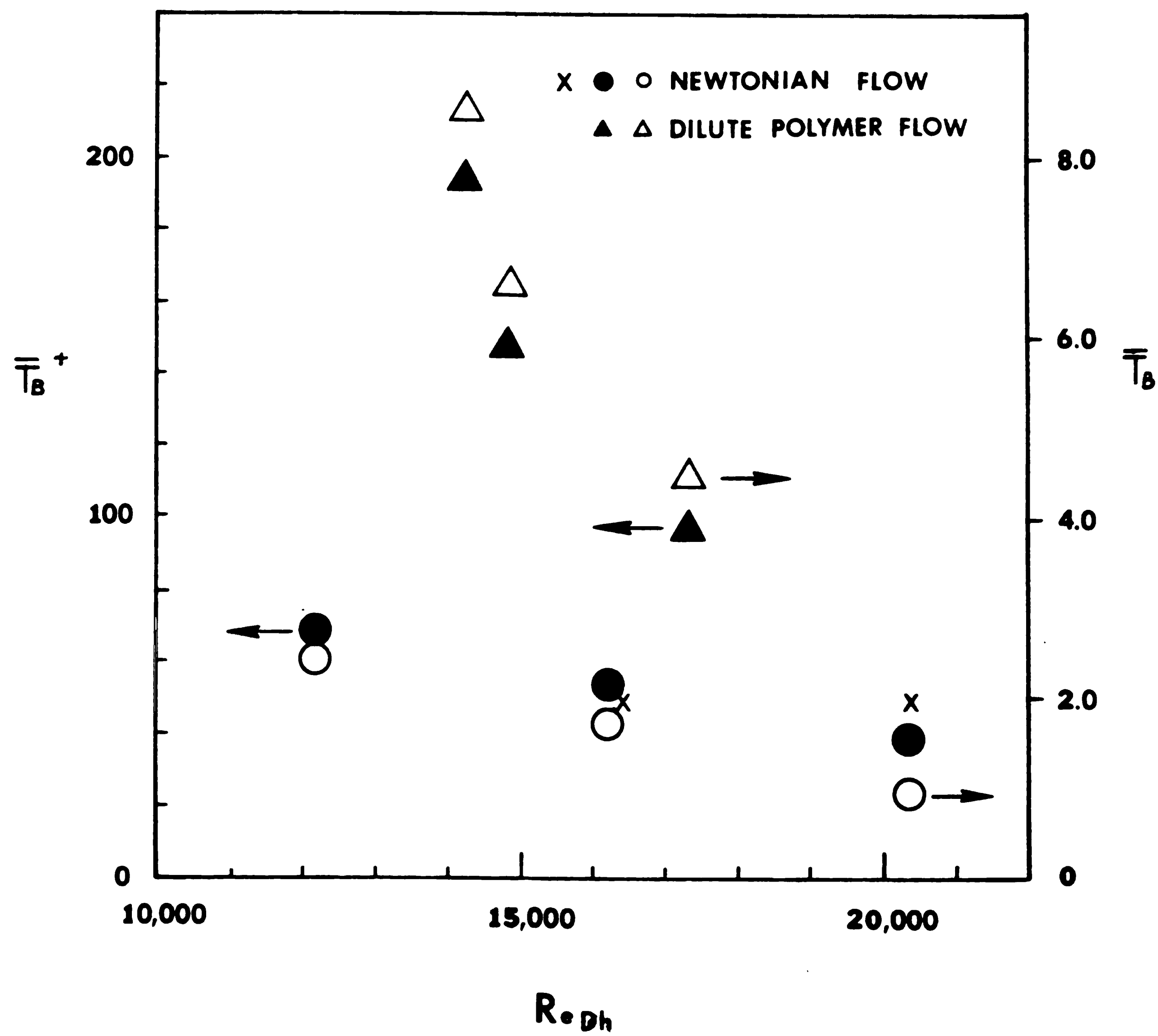

FIGURE 3.6 **TIME SCALE OF POCKETS**

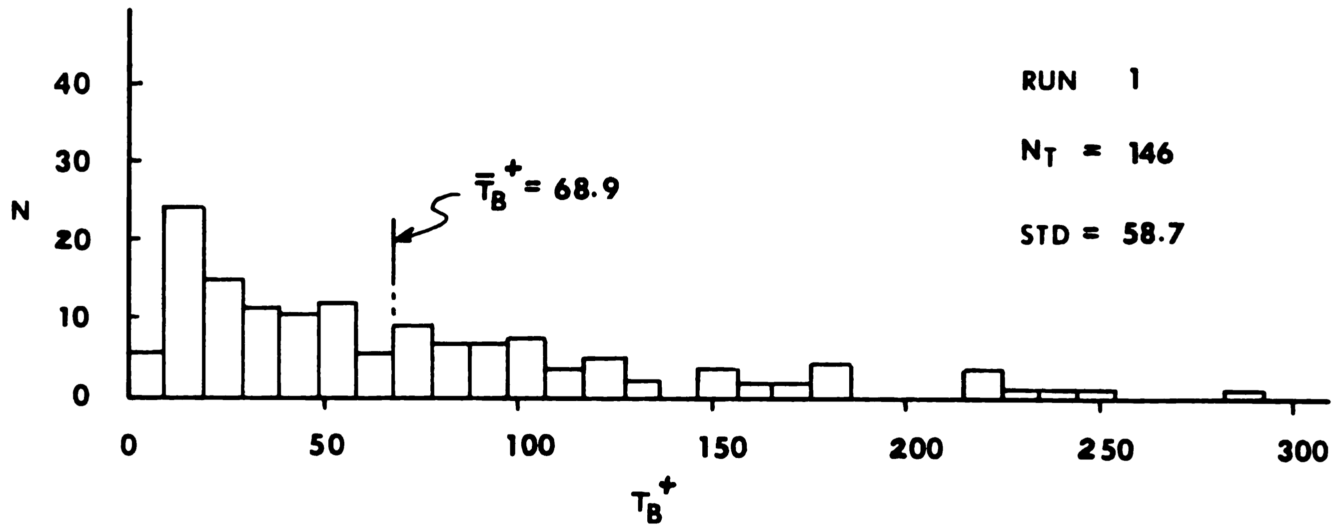

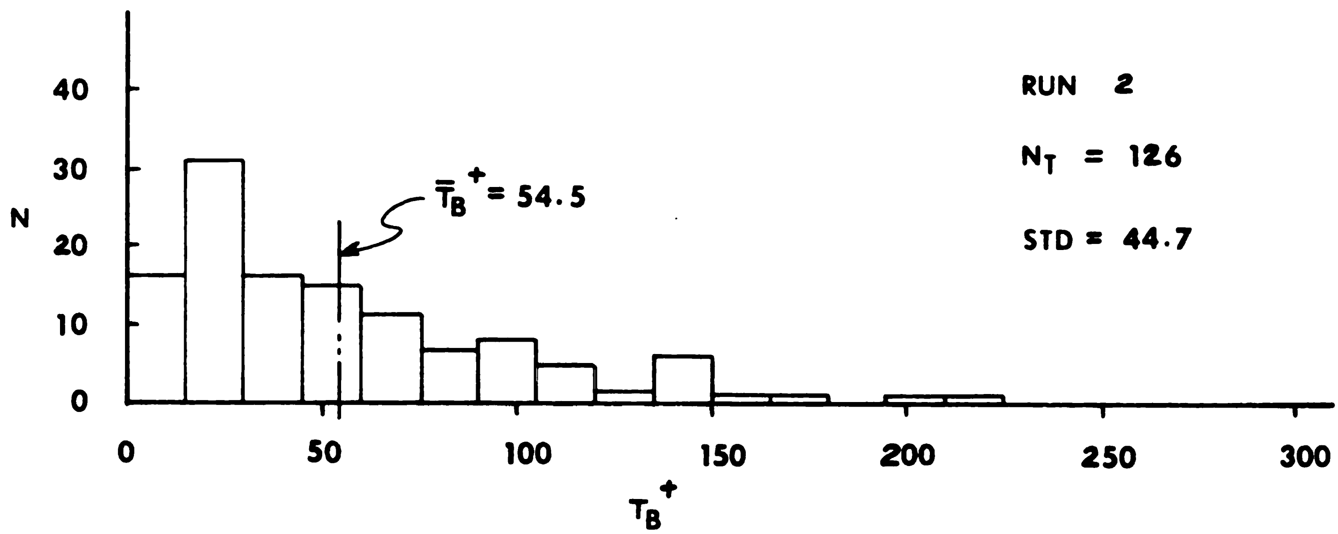

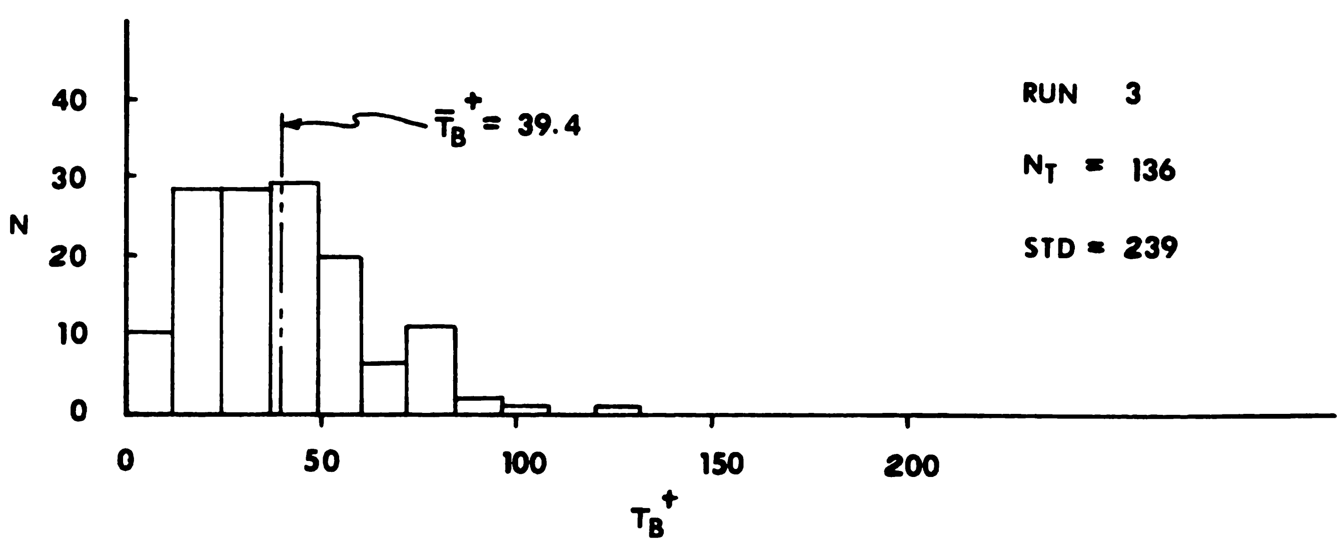

FIGURE 3.7(A) **HISTOGRAM OF TIME SCALE OF POCKETS**

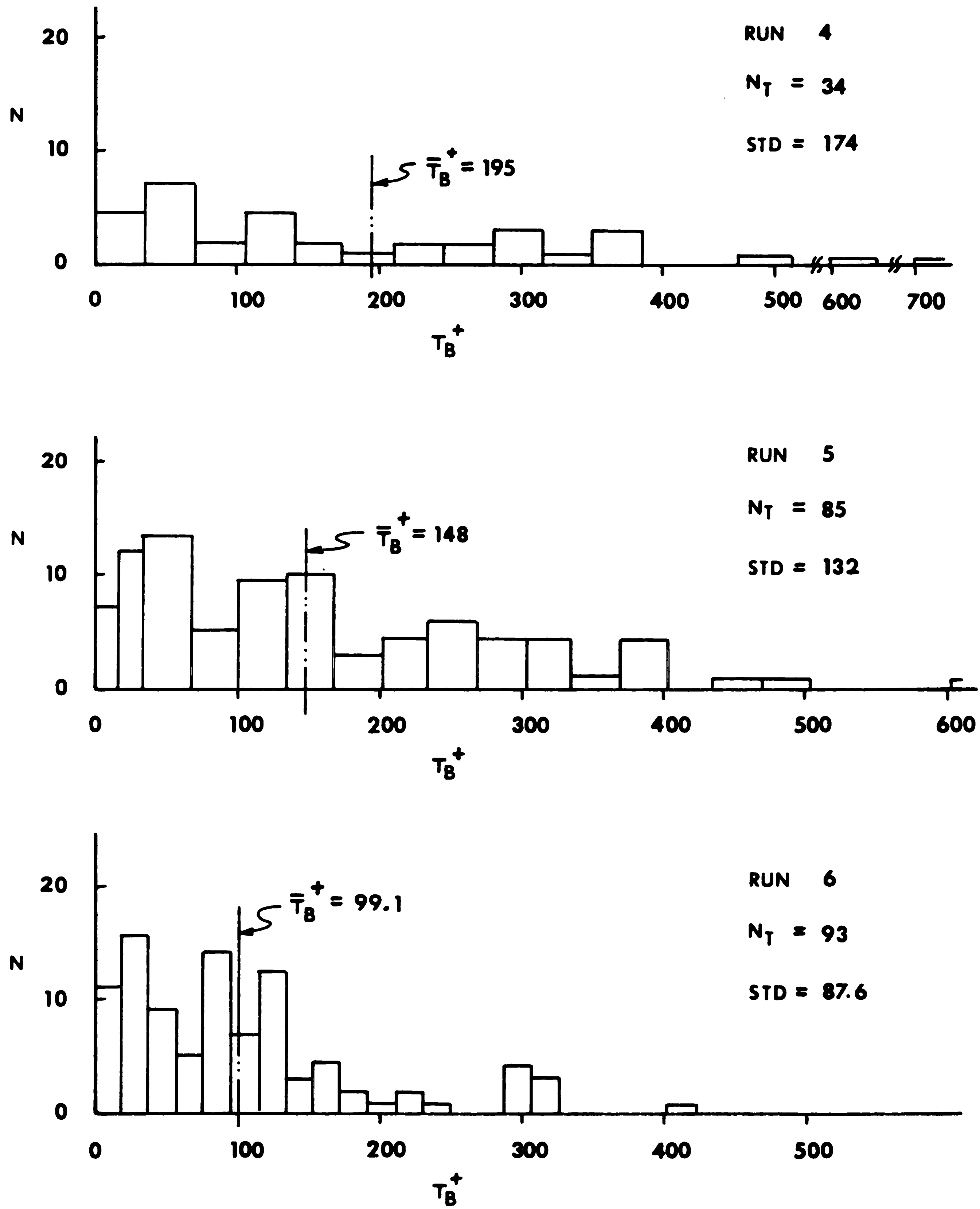

FIGURE 3.7 (B) **HISTOGRAM OF TIME SCALE OF POCKETS**

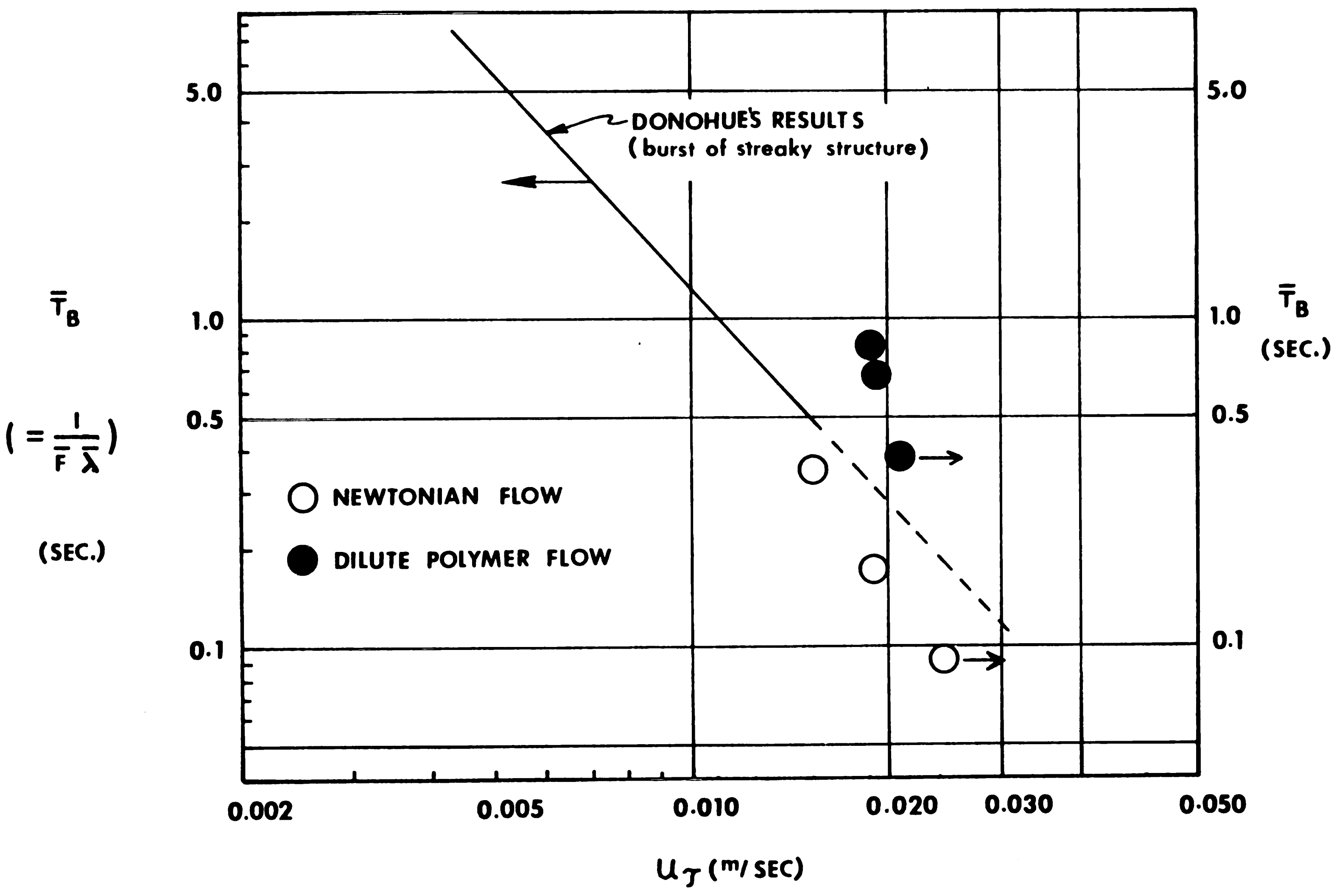

FIGURE 4.1 **AVERAGE TIME BETWEEN BURSTS**

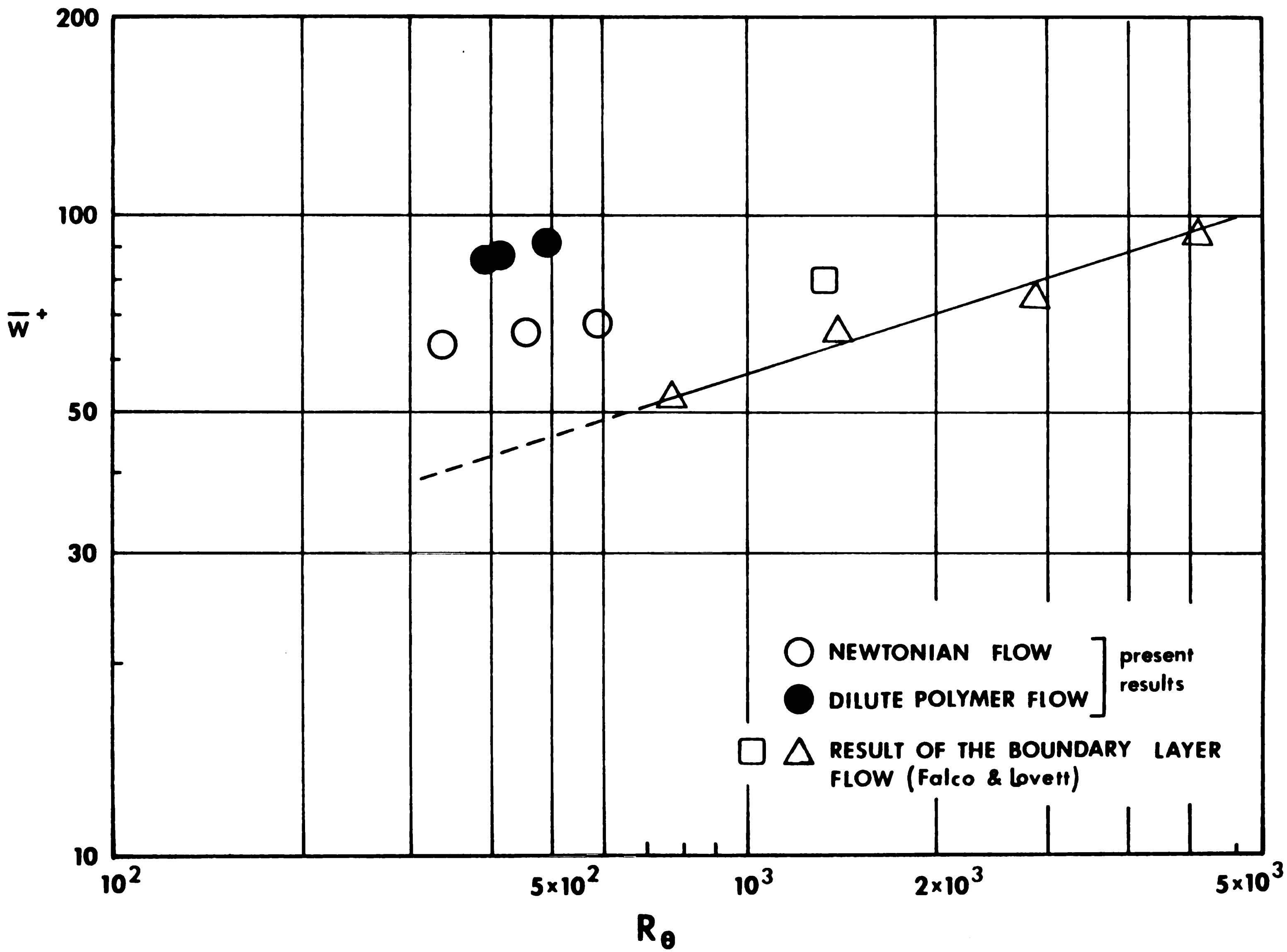

FIGURE 4.2 **COMPARISON OF LENGTH SCALE OF POCKETS**

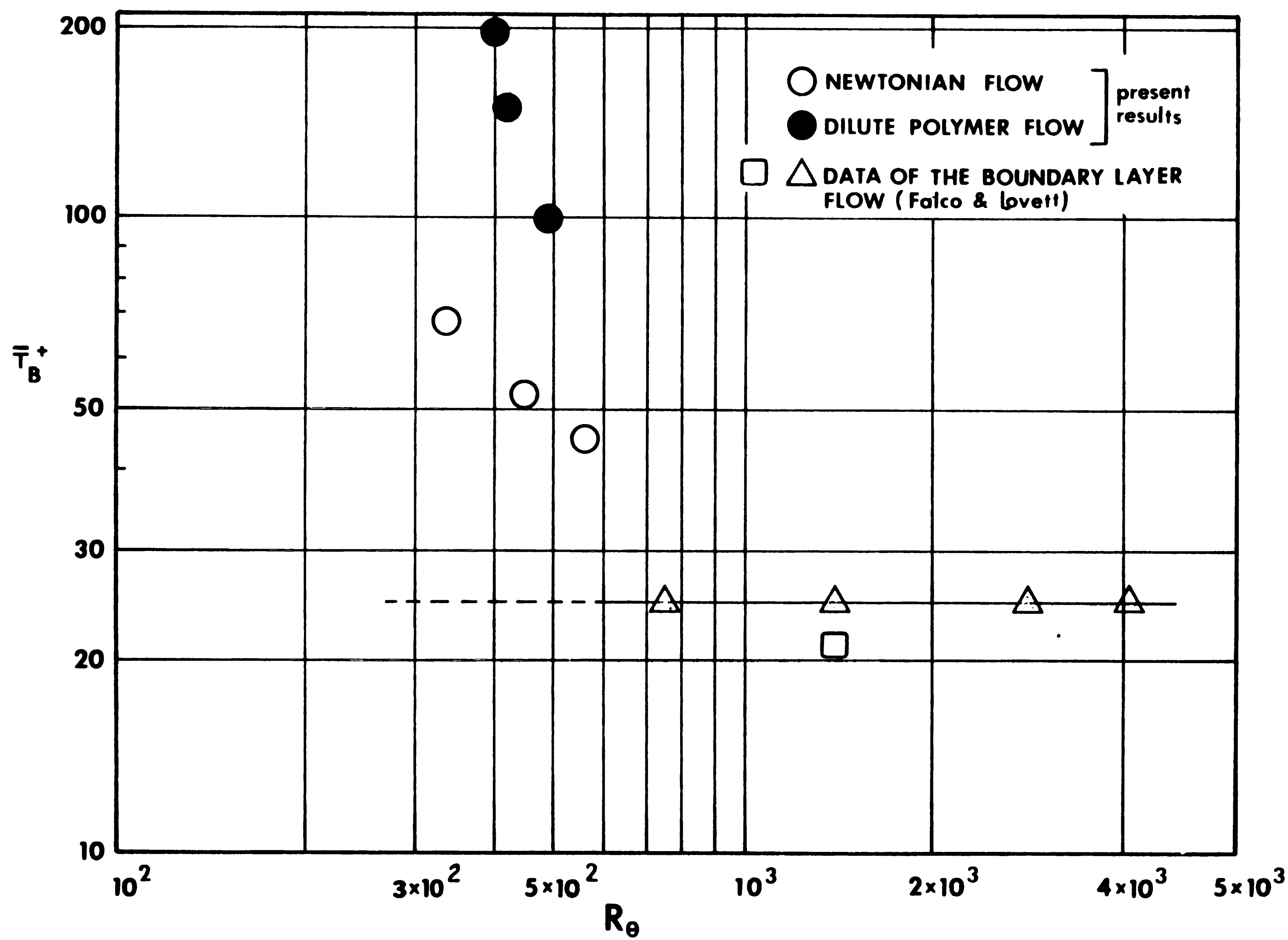

FIGURE 4.3 **COMPARISON OF TIME SCALE OF POCKETS**

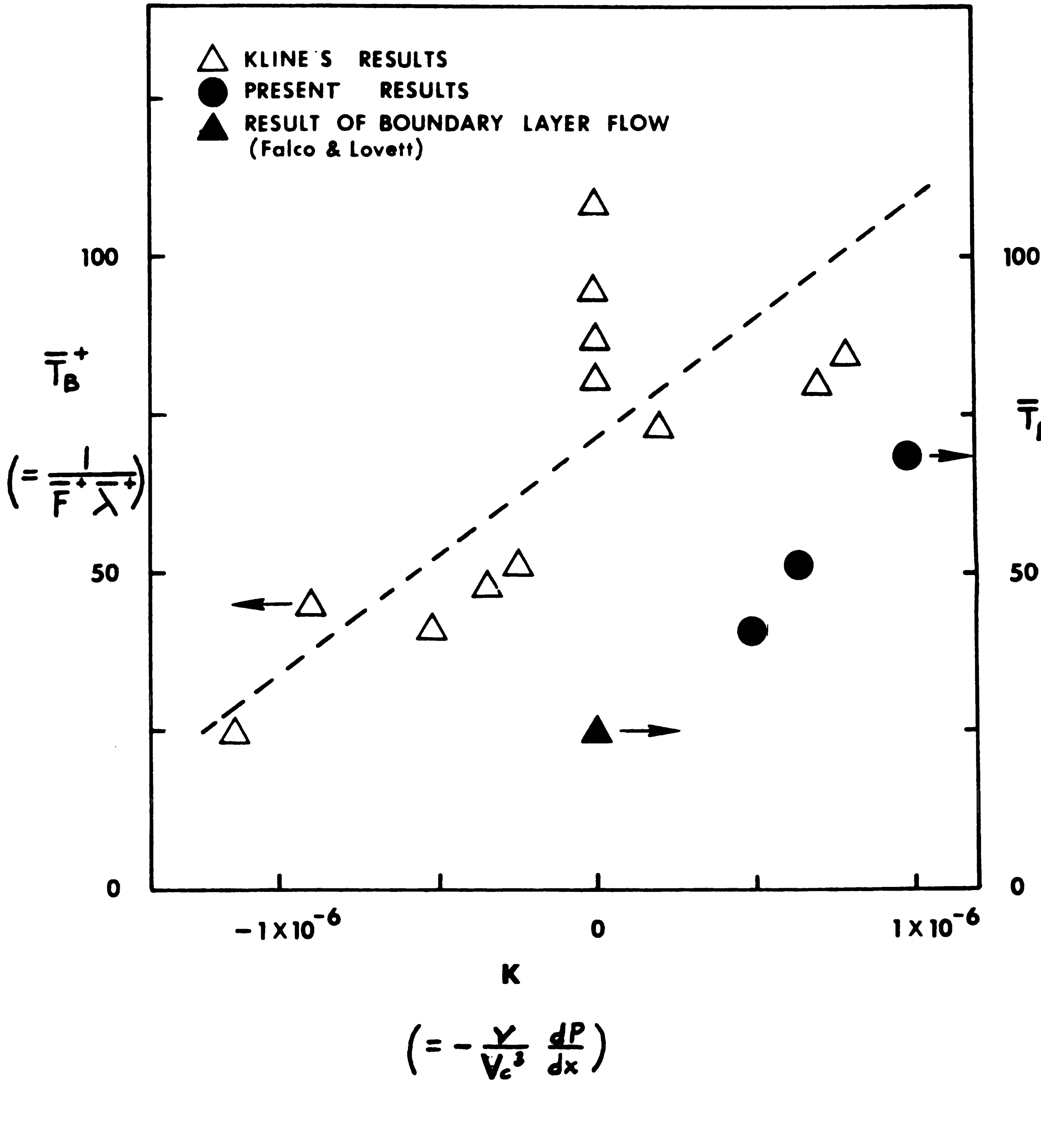

FIGURE 4.4 **EFFECTS OF PRESSURE GRADIENT ON TIME SCALE OF POCKETS**